frontiers | Frontiers in Cellular Neuroscience

TYPE Original Research
PUBLISHED 30 November 2023
DOI 10.3389/fncel.2023.1306006

Check for updates

OPEN ACCESS

EDITED BY
Takeshi Yoshimatsu,
Washington University in St. Louis,
United States

REVIEWED BY
Ivan Anastassov,
San Francisco State University, United States
Tomomi Ichinose,
Wayne State University, United States

*CORRESPONDENCE
Catherine W. Morgans
✉ morgansc@ohsu.edu

RECEIVED 02 October 2023
ACCEPTED 02 November 2023
PUBLISHED 30 November 2023

CITATION
Wakeham CM, Shi Q, Ren G, Haley TL, Duvoisin RM, von Gersdorff H and Morgans CW (2023) Trophoblast glycoprotein is required for efficient synaptic vesicle exocytosis from retinal rod bipolar cells. *Front. Cell. Neurosci.* 17:1306006. doi: 10.3389/fncel.2023.1306006

COPYRIGHT
© 2023 Wakeham, Shi, Ren, Haley, Duvoisin, von Gersdorff and Morgans. This is an open-access article distributed under the terms of the Creative Commons Attribution License (CC BY). The use, distribution or reproduction in other forums is permitted, provided the original author(s) and the copyright owner(s) are credited and that the original publication in this journal is cited, in accordance with accepted academic practice. No use, distribution or reproduction is permitted which does not comply with these terms.

# Trophoblast glycoprotein is required for efficient synaptic vesicle exocytosis from retinal rod bipolar cells

Colin M. Wakeham[1], Qing Shi[1], Gaoying Ren[1], Tammie L. Haley[1], Robert M. Duvoisin[1], Henrique von Gersdorff[1,2,3] and Catherine W. Morgans[1]*

[1]Department of Chemical Physiology and Biochemistry, Oregon Health and Science University, Portland, OR, United States, [2]Vollum Institute, Oregon Health and Science University, Portland, OR, United States, [3]Casey Eye Institute, Oregon Health and Science University, Portland, OR, United States

**Introduction:** Rod bipolar cells (RBCs) faithfully transmit light-driven signals from rod photoreceptors in the outer retina to third order neurons in the inner retina. Recently, significant work has focused on the role of leucine-rich repeat (LRR) proteins in synaptic development and signal transduction at RBC synapses. We previously identified trophoblast glycoprotein (TPBG) as a novel transmembrane LRR protein localized to the dendrites and axon terminals of RBCs.

**Methods:** We examined the effects on RBC physiology and retinal processing of TPBG genetic knockout in mice using immunofluorescence and electron microscopy, electroretinogram recording, patch-clamp electrophysiology, and time-resolved membrane capacitance measurements.

**Results:** The scotopic electroretinogram showed a modest increase in the b-wave and a marked attenuation in oscillatory potentials in the TPBG knockout. No effect of TPBG knockout was observed on the RBC dendritic morphology, TRPM1 currents, or RBC excitability. Because scotopic oscillatory potentials primarily reflect RBC-driven rhythmic activity of the inner retina, we investigated the contribution of TPBG to downstream transmission from RBCs to third-order neurons. Using electron microscopy, we found shorter synaptic ribbons in TPBG knockout axon terminals in RBCs. Time-resolved capacitance measurements indicated that TPBG knockout reduces synaptic vesicle exocytosis and subsequent GABAergic reciprocal feedback without altering voltage-gated $Ca2^{+}$ currents.

**Discussion:** TPBG is required for normal synaptic ribbon development and efficient neurotransmitter release from RBCs to downstream cells. Our results highlight a novel synaptic role for TPBG at RBC ribbon synapses and support further examination into the mechanisms by which TPBG regulates RBC physiology and circuit function.

KEYWORDS

**rod bipolar cell, retina, synaptic transmission, trophoblast glycoprotein (TBPG), protein kinase C alpha (PKCa), ribbon synapse, electroretinogram (ERG), capacitance measurements**

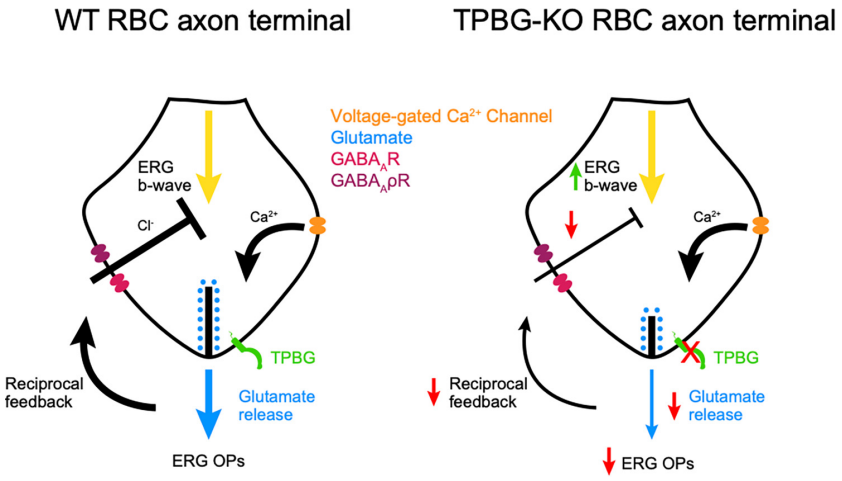


GRAPHICAL ABSTRACT

Proposed model for the effects of TPBG-KO on synaptic vesicle exocytosis and reciprocal feedback in RBC axon terminals. **(Left)** In a WT RBC, membrane depolarization opens voltage-gated $Ca2^{+}$ channels. The influx of $Ca2^{+}$ triggers vesicle exocytosis and glutamate release into the synaptic cleft. This glutamate is detected by downstream AII-ACs and A17-ACs. The A17-AC then releases GABA into the synaptic cleft which hyperpolarizes the RBC. **(Right)** In a TPBG-KO RBC, $Ca2^{+}$ influx is normal. However, in the absence of TPBG, synaptic vesicle exocytosis is reduced, resulting in reduced ERG OPs and reciprocal feedback.

## Introduction

Rod bipolar cells (RBCs) receive light-dependent synaptic input from rod photoreceptors in the outer plexiform layer (OPL) and drive retinal output by synapsing with AII amacrine cells (AII-ACs) in the inner plexiform layer (IPL). As the only dedicated bipolar cell in the primary rod visual pathway, RBCs must be able to reliably transmit visual signals over the whole range of rod sensitivity. Accurate transmission of light signals requires precise synaptic targeting and tight control of signal transduction between RBCs and its synaptic partners. Identifying and characterizing the proteins required for the optimization and regulation of RBC synaptic development and function is essential for expanding our understanding of how RBCs contribute to vision.

Leucine-rich repeat (LRR) proteins form a large class of transmembrane proteins, each containing multiple leucine-rich motifs arranged to form extracellular protein binding domains (Kobe and Deisenhofer, 1994; Kobe and Kajava, 2001). Several LRR proteins identified in RBCs have been implicated in the development and maintenance of synaptic morphology and function. At synapses between photoreceptors and ON-bipolar cells, LRIT3 and nyctalopin are required for the localization of signal transduction components to the post-synaptic compartment (Cao et al., 2011; Pearring et al., 2011; Neuillé et al., 2015, 2017; Hasan et al., 2019, 2020). In RBC dendrites, LRRTM4 forms a trans-synaptic complex with rod spherules (Agosto and Wensel, 2020), whereas in RBC axon terminals, LRRMT4 is required for functional GABA receptor clustering, reciprocal feedback inhibition, and dyad synapse formation (Sinha et al., 2020). The ELFN family of LRR proteins form trans-synaptic complexes between photoreceptors and bipolar cells without which functioning connections fail to develop and retinal circuitry is mis-wired (Cao et al., 2015, 2020).

We recently identified trophoblast glycoprotein [TPBG, also called 5T4 or WAIF1 (Wnt-activated inhibitory factor 1)] in a phosphoproteomics screen as a novel LRR transmembrane glycoprotein in mouse RBCs that undergoes PKCα-dependent phosphorylation (Wakeham et al., 2019). TPBG contains eight N-terminal extracellular LRR motifs and a short intracellular C-terminal tail with a PDZ-interacting domain (Zhao et al., 2014). TPBG immunofluorescence localizes to RBC dendrites, where it partially overlaps with GPR179 labeling, and is also present in RBC synaptic terminals, where it co-localizes with PKCα (Wakeham et al., 2020). Furthermore, its expression is closely linked to eye opening and TRPM1 expression, suggesting that TPBG may play a role in RBC development or physiology (Wakeham et al., 2020).

Because the role of TPBG in the retina has not been established, we sought to characterize the effects of genetic knockout of TPBG in mouse RBCs using immunofluorescence confocal microscopy, electron microscopy, and electrophysiological techniques. RBC synapses form specialized active zones, each containing a synaptic ribbon, that permit a greater bandwidth of information transfer than conventional synapses. Ribbon synapses are noted for tight vesicle-$Ca^{2+}$ coupling and a large supply of readily-available synaptic vesicles tethered close to the active zone (Morgans, 2000; Tom Dieck and Brandstätter, 2006; Moser et al., 2020). In this study, we report that TPBG is required for normal synaptic ribbon morphology and efficient synaptic vesicle exocytosis at RBC synapses, implicating TPBG in ribbon synapse development and function.

## Materials and methods

### Animals and statistical analysis

Constitutive TPBG knockout (TPBG-KO; KO) mice were B6;129S5-Tpbg$^{TM1Lex}$/Mmucd (MMRRC; UC Davis; Davis, CA, USA; Cat# 031630-UCD; RRID:MMRRC_031630-UCD). KO mice were purchased as cryopreserved sperm and reconstituted into a C57BL/6J (The Jackson Laboratory; Bar Harbor, M; Cat# 000664;

RRID:IMSR_JAX:000664) background. Age-matched homozygous wild type (WT) littermates were used as controls. We used mice of both sexes and all mice were maintained on a 12-h light/dark cycle and provided food and water *ad libitum*. Animals for immunofluorescence and electroretinogram experiments were 3–6 months old while animals used for patch clamp electrophysiology experiments were 3 months old. At least three mice were used from each condition for each experiment except for electron microscopy, which used one block per genotype. All animal procedures were in accordance with the National Institutes of Health guidelines and approved by the Oregon Health and Science University Institutional Animal Care and Use Committee.

Statistical analyses were performed in Prism 9 (GraphPad; San Diego, CA, USA) and reported as mean ± SEM. We detected significance between conditions using unpaired Welch's *t*-tests and Brown-Forsythe ANOVA tests when appropriate. Statistical significance is noted by asterisks [not significant (ns): $p > 0.05$; $^{*}p < 0.05$; $^{**}p < 0.01$; $^{***}p < 0.001$; $^{****}p < 0.0001$].

## Immunofluorescence

Fresh eyecups were prepared from dissected eyes by cutting behind the ora serrata and removing the cornea and lens. For sectioning, eyecups were fixed for 30 min by immersion in fresh 4% paraformaldehyde (PFA) in PBS. The fixed eyecups were washed in PBS and then cryoprotected via sequential immersion in 10, 20, and 30% sucrose in PBS. Sections were cut at 20 μm thickness. Retina sections were post-fixed for 10 min in 4% PFA, blocked and permeabilized by incubation at room temperature for 1 h in antibody incubation solution (AIS; 3% normal horse serum, 0.5% Triton X-100, 0.025% $NaN_3$ in PBS), and then incubated in primary antibodies diluted in AIS for 1 h at room temperature. After washing with PBS, the sections were incubated in secondary antibodies diluted in AIS for 1 h at room temperature. The slides were washed again in PBS and then mounted with VECTASHIELD PLUS antifade mounting media with DAPI (Vector Laboratories; Cat# H-2000-10).

For whole mount immunofluorescence, eyecups were fixed for 45 min by immersion in fresh 4% PFA in PBS. The fixed eyecups were washed in PBS then retinas were removed prior to blocking and permeabilization for 1 h in AIS. The retinas were incubated in primary antibodies diluted in AIS for 4 days at 4°C then washed overnight in PBST (PBS + 0.05% Triton X-100) at 4°C. Retinas were incubated in secondary antibodies diluted in AIS overnight at 4°C then washed again in PBST. Finally, the retinas were mounted with VECTASHIELD PLUS antifade mounting media.

Immunofluorescence images were taken with a Leica TCS SP8 X confocal microscope (Leica Biosystems; Wetzlar, Germany) using a Leica HC PL APO CS2 63x/1.40 oil immersion objective (Leica; Cat# 15506350). Brightness and contrast were adjusted equally across genotypes using Fiji (Schindelin et al., 2012). A Gaussian blur using a radius of 0.5 pixels was used to remove graininess from images. See figure legends for specific information on Z-step distance and number of steps. To compare the spatial relationship between presynaptic and postsynaptic proteins in the OPL, ROI lines were drawn across $Ca_v1.4$-GPR179 pairs and the intensity of both fluorescent channels was plotted against the line length in Fiji. The distance between the two fluorescence peaks approximates the distance across the synapse. To examine fluorescent puncta in RBC axon terminals in the IPL, PKCα binaries were created in Fiji using default auto-thresholds to isolate RBC axon terminals. These binaries were then merged with the other channels to remove PKCα-negative puncta. Fluorescent puncta were counted in PKCα-positive axon terminals and normalized to axon terminal area. Mander's colocalization coefficients were calculated using the JACoP plugin in Fiji to compare colocalization patterns between $Ca_v1.4$ and RIBEYE puncta after thresholding with Otsu's method. The M1 coefficient was used for the fraction of $Ca_v1.4$ containing RIBEYE and the M2 coefficient was for the fraction of RIBEYE containing $Ca_v1.4$. Colocalization of puncta in PKCα-negative areas was also calculated as a control.

## Immunoblotting

Retinas were extracted from freshly dissected eyes, suspended in chilled lysis buffer (50 mM Tris pH 7.4, 150 mM NaCl, 1 mM EDTA, 1% Triton X-100, 1% deoxycholate, 0.1% SDS) with 1X protease/phosphatase inhibitor cocktail (Cell Signaling Technology; Danvers, MA, USA; Cat# 5872) and homogenized with a Teflon-glass homogenizer. The lysate was centrifuged for 15 min at 16,400 rpm and 4°C, and the pellet was discarded. Retinal lysates were diluted to a protein concentration of 1 μg/μl in lysis buffer and brought to 1X NuPAGE LDS Sample Buffer (Thermo Fisher Scientific; Cat# NP0007) and 1X NuPAGE Sample Reducing Agent (Thermo Fisher Scientific; Cat# NP0009). Pre-cast NuPAGE 1 mm 4–12% Bis-Tris gels (Thermo Fisher Scientific; Cat# NP0322BOX) were loaded and run at 200 V and 140 mA for 55 min in 1X NuPAGE BOLT SDS Running Buffer (Thermo Fisher Scientific; Cat# B0001).

Proteins were transferred onto PVDF membranes using a wet transfer system and 1X NuPAGE Transfer Buffer (Thermo Fisher Scientific; Cat# NP00061) with 5% MeOH at 300 mA for 2 h. The membranes were then rinsed with methanol and blocked for 1 h in Odyssey Blocking Buffer TBS (LI-COR Biosciences; Cat# 927-50003) on a shaker at room temperature, before being incubated in primary antibody diluted in Odyssey buffer at 4°C overnight. The membranes were washed in TBST (Tris-buffered saline with 0.1% Tween-20), then incubated in secondary antibody diluted in Odyssey buffer for 1 h at room temperature before being washed in TBST. Dried blots were imaged using a LI-COR Odyssey CLx Imaging System at 680 and 800 nm.

## Electron microscopy

Mice were euthanized and enucleated and the retinas were quickly dissected and fixed for 30 min by immersion in 3% PFA and 1% glutaraldehyde. The tissue was then processed for electron microscopy using the Dresden protocol (Paridaen et al., 2013). Three-dimensional data was acquired using the Helios G3 NanoLab DualBeam FIB-SEM as previous described. Briefly, the resin blocks were trimmed to contain the ganglion cell layer and the IPL near the top edge of the block, mounted to a 45° pre-tilted stub, and coated with 8 nm of carbon. A focused beam of

gallium atoms ablated 4 nm off the surface of the sample (FIB conditions: 30 keV accelerating voltage, 790 pA beam current) over the SEM imaging area of 25 μm x 10 μm. The freshly ablated surface was then imaged by backscattered electrons using the In-Column Detector (SEM conditions: 3 keV accelerating voltage, 400 pA beam current, 4 nm per pixel, 3 μs dwell time; image resolution: 6144 × 4086, 4 nm isotropic). Ablation and imaging cycles were run over a 3-day period resulting in a sample depth of roughly 5 μm (1,373 images for the WT dataset and 1,284 images for the TPBG-KO dataset). Image stacks were registered using Linear Stack Alignment with the SIFT algorithm in Fiji and cropped to remove alignment artifacts. RBC synaptic terminals were identified by their morphology (size, shape, presence of synaptic ribbons, and arrangement of postsynaptic elements) and their proximity to the ganglion cell layer.

## Electroretinogram recording

Mice were dark-adapted overnight and prepared for recording under dim red light. Anesthesia was initiated via IP injection of ketamine:xylazine (100:10 mg/kg) and maintained with booster injections (30:3 mg/kg) at approximately 30 min intervals until completion of the experiment. Body temperature was maintained at 36.5–38°C. Before recording, the pupils were dilated with 2.5% phenylephrine and 1% tropicamide, and the cornea was anesthetized with 1% topical proparacaine. A wire loop placed under the upper teeth was used to draw the mouse into a custom-made holder that stabilized the head and permitted delivery of 95% $O_2$/5% $CO_2$ (carbogen; ~0.25 l/min). The recording was made using a custom contact lens electrode featuring a central platinum wire placed against the cornea with a small drop of hypromellose to prevent drying. A loop electrode placed behind the eye served as a reference electrode and a needle electrode placed in the tail served as a ground. The mice were placed in a Ganzfeld sphere and light stimuli were provided by custom 502 nm LED photostimulators. Light stimulus intensity was controlled with neutral density filters and by altering flash duration and was measured *post hoc* with an ILT5000 radiometer (International Light; Newburyport, MA; USA) using a scotopic filter. Traces were recorded with customized software (ERGLab; Richard Weleber; Casey Eye Institute; Portland, OR, USA).

Full-field scotopic electroretinograms (ERGs) from both eyes were recorded simultaneously after a series light flashes ranging from $8.71 \times 10^{-1}$ to $8.51 \times 10^{1}$ cd·s/m$^2$ [−0.06 to 1.93 log(cd·s/m$^2$)] (Xiong et al., 2015). For dimmer intensities [−1 to 0 log(cd·s/m$^2$)], three trials were averaged with inter-flash intervals of 20 s. For brighter intensities [0 to 2 log(cd·s/m$^2$)], two trials were averaged with inter-flash intervals of 30–120 s.

ERGLab data was exported for offline processing using a custom Python script and the SciPy package.[1] Statistical analyses were performed in Prism 9 (GraphPad; San Diego, CA, USA). The start of the flash stimulus was set to time zero and traces were baselined. A-waves and b-waves were isolated using a low-pass filter (60 Hz) and OPs were isolated with a Butterworth band-pass filter (30–300 Hz) and the "signal.filtfilt" function in SciPy (**Supplementary Figure 1**). The a-wave amplitudes were measured from baseline-to-trough, b-wave amplitudes were measured from a-wave trough-to-b-wave peak, and the b/a-wave ratio was calculated to normalize responses. OP amplitude was measured from trough-to-peak of the largest wave and the OP/b-wave ratio was calculated using b-wave amplitudes from the same recording.

## Patch clamp electrophysiology

Retinas were isolated and embedded in 3% low melting point agarose (Sigma; Cat# A0701) in carbogenated bicarbonate-buffered Ames medium (Ames and Nesbett, 1981; Ames Medium w/L-Glutamate; US Biological; Swampscott, MA, USA; Cat# A1372-25) and 200–250 μm slices were prepared with a Leica VT1200 vibrating microtome. For chemically simulated light response experiments, retinas were sliced in carbogenated Ames. For all other recordings, slicing was performed in chilled and carbogenated low-$Na^+$, high-sucrose cutting solution containing (in mM): 210 sucrose, 35 $NaHCO_3$, 20 HEPES, 10 glucose, 6 $MgCl_2$, 3 sodium pyruvate, 2.5 KCl and 0.5 $CaCl_2$ and buffered to pH 7.4 with NaOH. Retina slices were stored at room temperature in carbogenated Ames medium before being transferred to the recording chamber. Heated (31–33°C) Ames medium was continuously perfused over the retinal slices during all patch-clamp recordings.

Thick-walled borosilicate glass pipettes (World Precision Instruments; Sarasota, Fl, USA; Cat# 1B150F-4) were pulled using a Narishige PP-830 electrode puller (Tokyo, Japan). Ultrapure salts were purchased from Sigma-Aldrich (St. Louis, MO, USA). For RBC visualization, the fluorescent tracer Alexa Fluor 594 Hydrazide (100 μM; Thermo Fisher Scientific; Cat# A10438) was added to the pipettes. Whole-cell voltage-clamp and current-clamp recordings were performed in photopic conditions using a double EPC-10 patch clamp amplifier controlled by Patchmaster software (HEKA Elektronik, Lambrecht/Pfalz, Germany) or an Axon Axopatch 200B controlled by pCLAMP software (Molecular Devices; San Jose, CA, USA). Data was acquired at a 20 kHz sampling rate and filtered with a 2.9 kHz low-pass Bessel filter. RBCs were targeted visually using Dodt gradient contrast microscopy and confirmed *post hoc* with cell-filling and epifluorescence microscopy. Both pCLAMP and Patchmaster data sets were exported to Igor Pro (WaveMetrics, Lake Oswego, OR, USA) for offline analysis with custom Igor scripts and statistical analysis was performed in Prism. We used a P/10 leak subtraction protocol (−80 mV to −73 mV) in voltage-clamp to isolate voltage-gated $Ca^{2+}$ currents and GABAergic feedback currents; leak traces for each trial were baselined, summated, and subtracted from the raw pulse trace.

To record chemically simulated light responses, pipettes were pulled to 10–12 MΩ and backfilled with a potassium gluconate solution containing (in mM): 125 K-gluconate, 8 KCl, 5 HEPES, 1 $MgCl_2$, 1 $CaCl_2$, 3 adenosine 5′-triphosphate magnesium salt (Mg-ATP), 0.5 guanosine 5′-triphosphate disodium salt ($Na_2$-GTP), and 5 EGTA, and pH was adjusted to 7.3 with KOH. The Ames medium was supplemented with 4 μM L-(+)-2-amino-4-phosphonobutyric acid (L-AP4), an mGluR6 agonist, to maintain a simulated dark-adapted state. A puffer pipette (12–18 MΩ) was maneuvered into the dendritic field of the target cell, and the cell was patched

1 https://docs.scipy.org/doc

in voltage-clamp and held at −60 mV. The mGluR6 antagonist (RS)-α-cyclopropyl-4-phophophenylglycine (CPPG) was applied directly to the dendrites using a Picospritzer II (Parker Hannifin; Hollis, NH, USA; 600 μM at 20 psi) for 5 s and the RBC response was recorded. For each cell, four sweeps were recorded at 15-s intervals.

For current-clamp experiments, pipettes were pulled to 9–12 MΩ and backfilled with a potassium gluconate solution containing (in mM): 104 K-gluconate, 10 KCl, 10 HEPES, 4 Mg-ATP, 0.4 $Na_2$-GTP, 10 $Na_2$-Phosphocreatine, and 2 EGTA, and pH was adjusted to 7.3 with KOH. The Ames medium was supplemented with 1 mM $CaCl_2$ and the synaptic blockers (in μM): 0.5 strychnine (glycine receptor blocker), 3 gabazine (SR 95531; $GABA_A$ receptor blocker), 50 [1,2,5,6-tetrahydropyridin-4-yl]methylphosphinic acid (TPMPA; $GABA_A\rho$ receptor blocker), and 4 L-AP4 to block excitatory and inhibitory inputs. The total external $CaCl_2$ concentration was estimated to be 2.15 mM. Cells were first patched in voltage-clamp and then the amplifier was switched to fast current-clamp mode using the EPC-10 Gentle CC-Switch feature. Resting membrane voltage was recorded at 0 pA and then current was injected for 100 ms from −80 pA to 80 pA in 20 pA steps. Peak voltage was measured as the peak (min or max) voltage immediately after the onset of the current pulse, and sustained voltage was measured as the average over the final 10 ms of the pulse. For each cell, five sets of sweeps were recorded at 5-s intervals.

For the remaining experiments, the pipettes were pulled to 5–8 MΩ and backfilled with a cesium gluconate solution containing (in mM): 94 Cs-gluconate, 10 HEPES, 20 tetraethyl ammonium chloride (TEA-Cl), 4 Mg-ATP, 0.4 $Na_2$-GTP, 10 $Na_2$-Phosphocreatine, and 2 EGTA, and pH was adjusted to 7.3 with CsOH.

For voltage-clamp time-resolved capacitance recordings, the Ames medium was supplemented with 1 mM $CaCl_2$ and (in μM): 0.5 strychnine, 3 gabazine, 50 TPMPA, and 4 L-AP4 to isolate voltage-gated $Ca^{2+}$ currents and maximize membrane resistance. Pipettes were wrapped with parafilm to reduce pipette capacitance and electrical noise. Membrane capacitance ($C_m$), membrane resistance ($R_m$), and series resistance ($R_s$) were measured using the "sine + DC" method implemented in Patchmaster software (Gillis, 2000; Oltedal and Hartveit, 2010; Balakrishnan et al., 2015). Exocytosis was evoked in voltage-clamp mode with a 100 ms depolarizing pulse from −80 mV to −10 mV to activate voltage-gated $Ca^{2+}$ currents. Resting $C_m$ was measured using a sinusoidal voltage command (200 Hz, 30 mV trough-to-peak) superimposed over the membrane holding potential (−80 mV) and one measurement was generated per cycle (**Figure 5A**). An increase in exocytosis ($\Delta C_m$) was measured from the change in $C_m$ values before and after the depolarizing pulse. A baseline was established by averaging the resting $C_m$ over the 1 s immediately preceding the voltage step. $C_m$ measurements immediately after repolarization were excluded from analysis to allow for the full decay of evoked conductances and $C_m$ was averaged over the following 500 ms. Cells were discarded if changes in $C_m$ correlated significantly with changes in $R_m$ or $R_s$. For each cell, five sets of sweeps were recorded with 15 s intervals. To remove noise, $C_m$ data was filtered through a 5 Hz low-pass FIR filter. When different frequency sinusoidal voltage commands were used, recordings were resampled to 200 Hz for ease of comparisons.

To record reciprocal inhibitory currents, the Ames medium was supplemented with 1 mM $CaCl_2$, 4 μM L-AP4, and 0.5 μM strychnine. Feedback current was evoked in voltage-clamp mode with a 100 ms depolarizing pulse from −80 mV to −10 mV to activate voltage-gated $Ca^{2+}$ currents and subsequent outward GABAergic inhibitory currents. We isolated inhibitory currents ($I_{Inhib}$) by subtracting recordings with GABA blockers ($I_{Ca}$) were from recordings without GABA blockers ($I_{Total}$), and calculated the charge transfer across the duration of the depolarizing pulse. Five sets of sweeps were recorded at 5-s intervals.

# Results

## TPBG is not required for normal gross RBC morphology

We used the constitutive Tpbg knockout mouse line B6;129S5-$Tpbg^{TM1Lex}$/Mmucd (referred to as TPBG-KO or KO) to analyze the consequences of genetic deletion of TPBG in the retina. Wild type (WT) littermates were used as controls. Expression and localization of TPBG were examined by western blotting and immunofluorescence confocal microscopy (**Figure 1**). As previously reported (Wakeham et al., 2020), the TPBG antibody labels RBC cell bodies, dendrites, and axon terminals in the WT retina, as well as a narrow band in the middle of the IPL corresponding to the processes of TPBG-expressing amacrine cells. TPBG immunoreactivity was absent throughout the KO retina (**Figure 1A**); this was confirmed by immunoblotting (**Figure 1B**) of WT and KO retinal lysates with the TPBG antibody using β-actin as a loading control. Using an antibody against PKCα in WT and TPBG-KO retina, we found no discernable disruption in morphology of RBC dendrites or axon terminals in KO retinas (**Figures 1C, D**).

## Genetic knockout of TPBG alters the scotopic ERG light response

The light response of RBCs is reflected in the b-wave of the dark-adapted (scotopic) full-field electroretinogram (ERG), a commonly-used technique for recording the electrical responses of the whole retina *in vivo*. Different components of the ERG waveform correspond to the activity of specific cell types in the retina. The a-wave is an initial negative deflection corresponding to hyperpolarization of the photoreceptors (Robson and Frishman, 2014), whereas the b-wave, a larger and slower positive deflection, primarily corresponds to the subsequent depolarization of the ON-bipolar cells (Stockton and Slaughter, 1989). Rod driven activity can be isolated by dark-adapting the mouse before testing; therefore, the dark-adapted ERG b-wave represents the activity of RBCs in response to light stimuli.

We recorded the scotopic ERG light responses in dark-adapted anesthetized WT (blue; $n$ = 12) and TPBG-KO (KO; orange; $n$ = 14) mice across several stimulus intensities, from dim [−0.06 log(cd·s/$m^2$)] to bright [1.93 log(cd·s/$m^2$)]. We applied a 60 Hz low-pass filter to remove oscillatory potential (OP) contamination from the ERG a- and b-waves, and a 30–300 Hz Butterworth

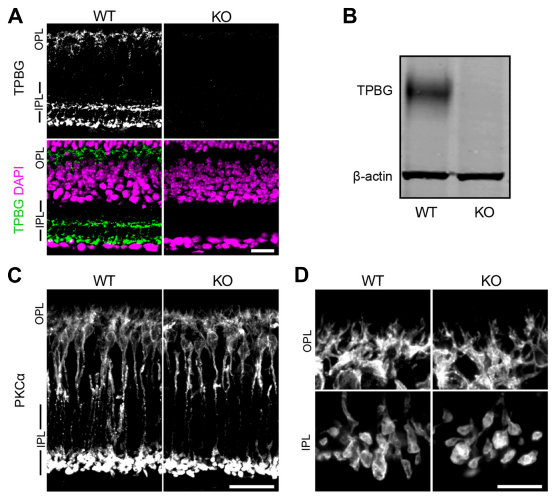


FIGURE 1
TPBG-KO does not alter gross RBC morphology.
**(A)** Immunofluorescence confocal microscopy of WT (left) and TPBG-KO (KO; right) retina sections labeled with an antibody against TPBG (green). The nuclear stain DAPI (bottom; magenta) was used to highlight the neuronal layers of the retina.
**(B)** Immunoblot of WT and TPBG-KO (KO) retinal lysates probed for TPBG and β-actin. The two channels were imaged separately and merged. **(C)** Confocal microscopy of WT (left) and TPBG-KO (KO; right) retina sections labeled with an antibody against PKCα.
**(D)** Close-up images depicting the OPL (top) and IPL (bottom) for better visualization. For all images, Z-projections of 11 sections were used with a Z-step distance of 0.415 μm for a total thickness of 4.57 μm. Intensity and contrast was adjusted equally across genotypes. OPL, outer plexiform layer; IPL, inner plexiform layer. Scale bars: **(A,C)** 20 μm; **(D)** 10 μm.

band-pass filter to isolate OPs for further analysis (Figure 2A). There was no difference in a-wave amplitudes across intensities (Supplementary Figure 1), indicating that the KO did not affect the rod photoreceptor light responses, but there was an enlarged b-wave in the TPBG-KO mouse (Figure 2B). Because the ERG b-wave is dependent on upstream photoreceptor activation, which is represented by the a-wave, it is common practice for ERG b-wave amplitudes to be normalized to a-wave amplitudes for comparison across animals. The TPBG-KO increased the normalized b-waves (b/a-wave ratio) across the range of stimuli intensities (Figure 2C), indicating a larger and more prolonged RBC light response in TPBG-KO mice.

Oscillatory potentials (OPs) are low amplitude, high frequency waves superimposed over the rising phase of the ERG b-wave and observed after bright stimuli. Previous studies indicate that OPs originate from rhythmic activity in the IPL downstream of the bipolar cells (Ogden, 1973). Because the light response of a dark-adapted retina is primarily rod-driven, the OPs are indirectly correlated to RBC output. Therefore, we normalized the OP amplitude by the b-wave amplitude (OP/b-wave ratio) of the corresponding ERG recording. Normalized TPBG-KO OPs were reduced compared to WT (Figures 2D, E). TPBG is primarily expressed in RBCs, therefore an effect of TPBG-KO on the OPs is most likely to be due to reduced RBC output onto downstream neurons, though an effect mediated by the TPBG-expressing amacrine cells cannot be ruled out.

## TPBG is not required for mGluR6-driven responses in RBC dendrites

We examined the expression and localization patterns of key pre- and post-synaptic proteins that are required for synaptic transmission between rod photoreceptors and RBCs. RBCs receive synaptic input from rod photoreceptors via a sign-inverting signal transduction cascade localized to the tips of RBC dendrites. Glutamate released from rod photoreceptors is detected by the group III metabotropic glutamate receptor mGluR6 (Nakajima et al., 1993; Masu et al., 1995; Vardi et al., 2000; Xu et al., 2012), that is negatively coupled to the TRPM1 cation channel (Morgans et al., 2009; Shen et al., 2009; Koike et al., 2010a,b). Thus, a light stimulus relieves TRPM1 tonic inhibition, permitting cation influx and subsequent RBC depolarization.

First, we looked at the spatial relationship between presynaptic elements in the rod spherule and the tips of the RBC dendrites (Figure 3A) using an antibody against the rod L-type $Ca^{2+}$ channel subunit $Ca_V1.4$ to label the horseshoe-shaped active zone and an antibody that labels GPR179 in RBC dendritic tips (Hasan et al., 2016). In normal rod-RBC synapses, GPR179 labeling appears as puncta within the concavity of the horseshoe-shaped $Ca_V1.4$ immunofluorescence. We quantified the spatial relationship between rod active zones and RBC dendritic tips by measuring the distance between the peak intensity for each fluorescent channel (Figure 3B). We found no difference between WT (blue; $n$ = 66 synapses) and TPBG-KO (KO; orange; $n$ = 54 synapses) synaptic distance [Figure 3C; WT: 0.43 ± 0.006 μm; KO: 0.43 ± 0.004 μm; Welch's $t$-test: $p$ = 0.96, $t(117.60)$ = 0.052], suggesting that RBC dendrites form morphologically normal invaginations into rod spherules in the TPBG-KO mouse.

Scotopic ERG recordings revealed increased b-waves in TPBG-KO mice (Figure 2) indicating an enhanced light response in KO RBCs. Because the RBC light response is initiated by TRPM1, we compared TRPM1 currents between WT (blue; $n$ = 10) and TPBG-KO (KO; orange; $n$ = 6) RBCs by recording chemically simulated light responses in retinal slices in whole-cell voltage-clamp (Figures 3D–F). In this technique, bath application of the mGluR6 agonist L-AP4 maintains the retina in a simulated dark-adapted state, and brief puffs of the mGluR6 antagonist, CPPG, onto the dendrites simulates a light flash and evokes TRPM1 currents (Figure 3D). TPBG-KO did not alter the CPPG-induced TRPM1 peak current [Figure 3E; WT: −88.24 ± 8.92 pA; KO: −98.04 ± 11.28 pA; Welch's $t$-test: $p$ = 0.51, $t(10.85)$ = 0.68] or charge transfer [Figure 3F; WT: −157.10 ± 47.01 pC; KO: −173.10 ± 38.62 pC; Welch's $t$-test: $p$ = 0.47, $t(12.40)$ = 0.74]. These results suggest that TPBG is not required for the formation of functional rod-RBC synapses and that the larger scotopic ERG b-waves do not reflect enhanced TRPM1 currents in the TPBG-KO.

## Synaptic ribbons are smaller in TPBG-KO RBCs compared to WT

Oscillatory potentials are thought to be generated by the inner retina, and RBCs drive the majority of downstream activity under scotopic conditions; thus, the attenuation of scotopic OPs in the TPBG-KO suggests a deficit in RBC output to third-order neurons.

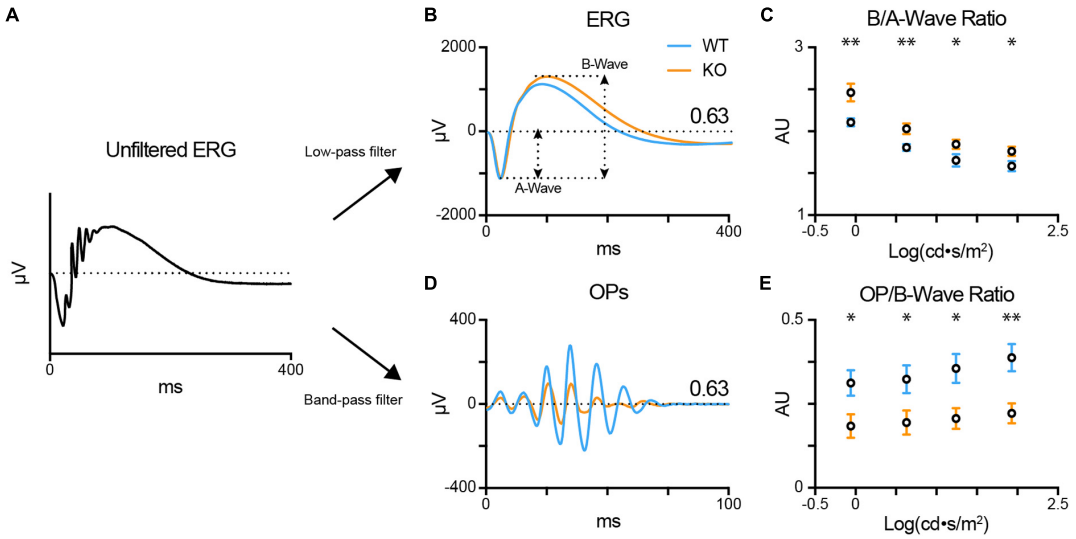


FIGURE 2
TPBG-KO alters the scotopic ERG after bright stimuli. Scotopic electroretinograms (ERGs) were recorded from dark-adapted WT (blue; $n$ = 12) and TPBG-KO (KO; orange; $n$ = 14) mice after light stimuli [−0.06 to 1.93 log(cd·s/m$^2$)]. **(A)** After baselining the raw, unfiltered ERG traces, a 60 Hz low-pass filter was used to remove OPs to better visualize the a- and b-waves. A 30–300 Hz Butterworth band-pass filter was used to isolate OPs from the ERG for quantification. **(B)** Average ERG recordings after light stimuli of 0.63 log(cd·s/m$^2$). A-wave amplitudes were measured from baseline to the a-wave trough and b-wave amplitudes were measured from the a-wave trough to the b-wave peak. **(C)** Quantification of b-wave amplitudes normalized to a-wave amplitudes. **(D)** Average oscillatory potentials (OPs) after light stimuli of 0.63 log(cd·s/m$^2$). **(E)** Quantification of OP amplitudes normalized to b-wave amplitudes. OP amplitudes were measured from the trough to peak of the largest wave. Quantified data is presented as the mean ± SEM. Statistical significance was determined using Welch's $t$-tests; *$p < 0.05$; **$p < 0.01$.

Like rods, RBCs signal to downstream cells using ribbon synapses. A depolarized potential entering the axon terminal prompts the opening of L-type voltage-gated $Ca^{2+}$ channels clustered beneath the ribbons and the resulting influx of $Ca^{2+}$ triggers the fusion (exocytosis) of ribbon-tethered synaptic vesicles (von Gersdorff et al., 1996). This process requires a close spatial relationship between the $Ca^{2+}$ channels the synaptic ribbons (Jarsky et al., 2010). We used triple immunofluorescence microscopy to examine the relative localization and expression patterns of the L-type $Ca^{2+}$ channel subunit, $Ca_v1.4$, and the primary structural synaptic ribbon protein RIBEYE (Figures 4A–C). Because neither $Ca_v1.4$ nor RIBEYE are specific to RBC axon terminals, we isolated RBC-specific immunofluorescence using a binary mask derived from PKCα immunofluorescence to exclude labeling from other bipolar cells in the IPL. $Ca_v1.4$ and RIBEYE show punctate immunofluorescence in RBC axon terminals and are co-localized or closely apposed (Figure 4A). Mander's overlap coefficients (M1 and M2) were calculated to examine colocalization between $Ca_v1.4$ and RIBEYE puncta in both control (PKCα-negative) terminals and RBC (PKCα-positive) terminals (Figure 4B). We found no differences in co-localization coefficients between WT and TPBG-KO control or RBC axon terminals: WT (blue; $n$ = 134 control puncta and 100 RBC puncta) and TPBG-KO (orange; $n$ = 327 control puncta and 119 RBC puncta), control M1 [WT: 0.53 ± 0.022 arbitrary units (AU); KO: 0.52 ± 0.013 AU; Welch's $t$-test: $p$ = 0.60, $t$(237.2) = 0.53], control M2 [WT: 0.40 ± 0.015 AU; KO: 0.42 ± 0.011 AU; Welch's $t$-test: $p$ = 0.28, $t$(288.1) = 1.09], RBC M1 [WT: 0.66 ± 0.016 AU; KO: 0.64 ± 0.015 AU; Welch's $t$-test: $p$ = 0.47, $t$(208.3) = 0.73], RBC M2 [WT: 0.32 ± 0.01 AU; KO: 0.31 ± 0.01 AU; Welch's $t$-test: $p$ = 0.76, $t$(216.9) = 0.31]. Additionally, we found that the number of ribeye puncta per unit area was unchanged in WT (blue; $n$ = 90 axon terminals) and TPBG-KO (KO; orange; $n$ = 109 axon terminals) RBC terminals [Figure 4C; WT: 2.07 ± 0.66 puncta/μm$^2$; KO: 2.03 ± 0.58 puncta/μm$^2$; Welch's $t$-test: $p$ = 0.70, $t$(177.8) = 3.92]. We saw no difference in synaptotagmin I/II immunofluorescence between RBC axon terminals in WT and TPBG-KO retinas [not shown; WT: 1.352 ± 0.0486 AU; KO: 1.446 ± 0.0560; Welch's $t$-test: $p$-value = 0.209, $t$(52.63) = 1.271].

To examine synaptic ribbons in RBC axon terminals, serial electron micrographs were collected from a volume each of WT and TPBG-KO retina using a focused ion beam scanning electron microscope (FIB-SEM). Bipolar cell terminals closest to the ganglion cell layer were identified as putative RBC axon terminals. The general ultrastructure of the RBC axon terminals, including the synaptic vesicles, synaptic ribbons, and postsynaptic elements was similar in WT and TPBG-KO retina. To estimate synaptic ribbon size, we measured the maximum distance that each ribbon extended into the cytoplasm from its attachment site on the plasma membrane in WT (blue; $n$ = 33 ribbons) and TPBG-KO (KO; orange; $n$ = 38 ribbons) and found that synaptic ribbons were 15% smaller in TPBG-KO RBCs compared to WT RBCs [Figure 4E; WT: 416.8 ± 13.78 nm; KO: 355.7 ± 8.85 nm; Welch's $t$-test: $p$ = 0.0004, $t$(55.65) = 3.74].

## TPBG is required for efficient exocytosis in RBC synaptic terminals

To examine the effect of TPBG-KO on RBC synaptic output, we recorded time-resolved membrane capacitance ($C_m$) before and after a depolarizing pulse using the "sine + DC"

10.3389/fncel.2023.1306006

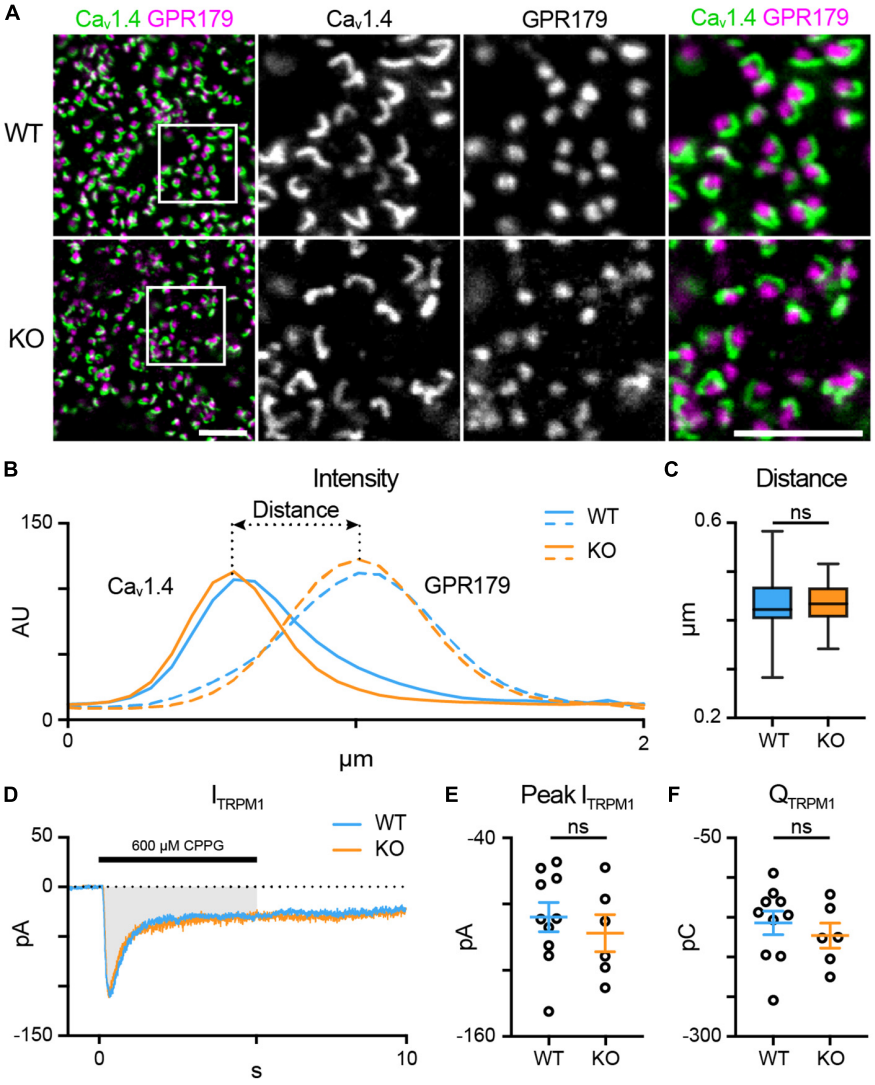


FIGURE 3
TPBG is not required for mGluR6-driven responses in RBC dendrites. **(A)** Immunofluorescence confocal microscopy from WT and TPBG-KO whole mount retinas using antibodies against the rod presynaptic calcium channel $Ca_V1.4$ (green) and the RBC post-synaptic protein GPR179 (magenta). Square boxes in the leftmost images indicate regions of interest expanded in the other images. Z-projections of two sections were used with a Z-step distance of 0.297 µm for a total thickness of 0.594 µm. Scale bar is 5 µm. **(B)** Plot of fluorescence intensity over distance from $Ca_V1.4$ (left) and GPR179 (right) channels from WT (blue; $n$ = 66 synapses) and TPBG-KO (KO; orange; $n$ = 54 synapses). **(C)** Quantification of synaptic distance. Box plot extends from the first to the third quartile and the whiskers extend across all points. The line in the box represents the median. **(D–F)** Chemically simulated light responses were recorded in WT (blue; $n$ = 10) and TPBG-KO (KO; orange; $n$ = 6) RBCs following a pulse of 600 µM CPPG for 5 s. **(D)** Example CPPG-induced TRPM1 currents. The gray bar represents the region across which charge transfer was calculated. **(E)** Quantification of peak CPPG-induced TRPM1 current ($I_{TRPM1}$) and **(F)** charge transfer ($Q_{TRPM1}$) over the 5-s duration of the CPPG pulse. For **E** and **F**, open circles represent single cells and colored bars represent the mean ± SEM. Statistical significance was determined using Welch's $t$-tests; ns: $p > 0.05$.

method (Gillis, 2000; Oltedal and Hartveit, 2010). High-resolution membrane capacitance changes ($\Delta C_m$) after a depolarizing pulse strongly correlate with vesicle exocytosis in neuroendocrine cells (Neher and Marty, 1982; Klyachko and Jackson, 2002) and glutamate release from bipolar cell axon terminals (Kim and von Gersdorff, 2016). A sinusoidal voltage command (200 Hz at 30 mV trough-to-peak) was superimposed over the holding voltage of −80 mV and exocytosis was evoked by depolarizing the cell to −10 mV to open the voltage-gated $Ca^{2+}$ channels (**Supplementary Figure 3A**). Membrane capacitance ($C_m$), membrane resistance ($R_m$), and series resistance ($R_s$) were recorded before and after the pulse and $\Delta C_m$ was measured as the change in $C_m$ after exocytosis. Changes in $R_m$ and $R_s$ were not correlated with changes in $C_m$ (**Supplementary Figure 3B**).

$C_m$ measurements in RBCs are complicated by the attenuation and filtering of the sinusoidal voltage command amplitude down their narrow axons (Oltedal et al., 2009; Oltedal and Hartveit, 2010). We sought to confirm that a low-frequency sinusoidal command reduces attenuation and maximizes RBC $C_m$ changes compared to higher frequencies (**Supplementary Figures 3C–F**) using 200 ($n$ = 6), 400 ($n$ = 4), 800 ($n$ = 4), and 1,600 ($n$ = 4) Hz commands. We found no difference in the voltage-gated $Ca^{2+}$ current amplitude ($I_{Ca}$) or charge transfer ($Q_{Ca}$) across frequencies (not shown), but the $\Delta C_m$ [**Supplementary Figures 3C, D**; 200 Hz: 41.94 ± 4.95

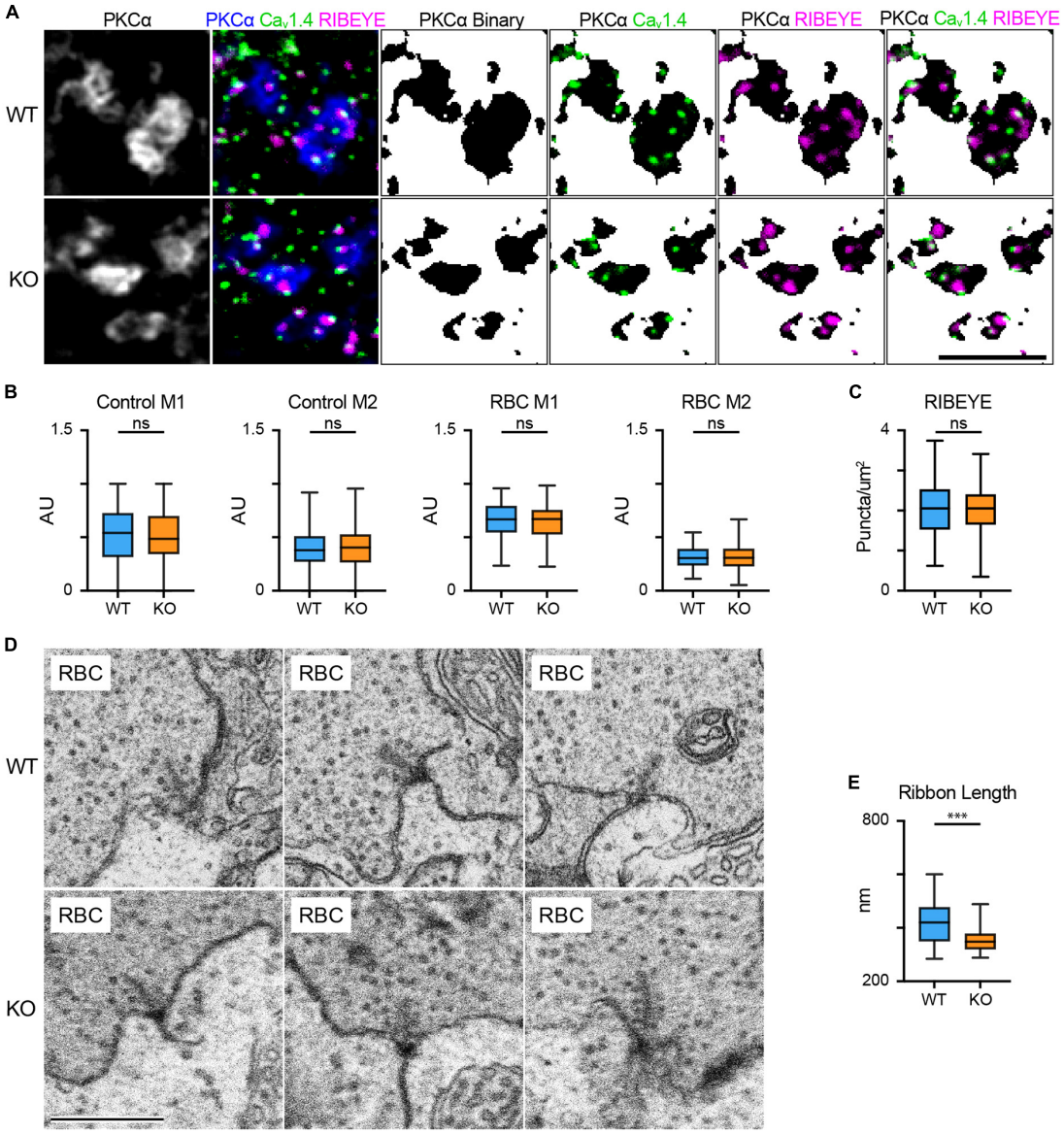


FIGURE 4
RBC synaptic ribbons are smaller in the TPBG-KO retina. **(A)** Triple immunofluorescence confocal microscopy of WT and TPBG-KO (KO) whole mount retinas using antibodies against PKCα (blue), $Ca_V1.4$ (Green) and RIBEYE (magenta). To isolate labeling in RBC axon terminals, binary images were created using the PKCα channel and overlayed over the other two channels to generate binary masks. Z-projections of two sections were used with a Z-step distance of 0.297 μm for a total thickness of 0.547 μm. The scale bar is 5 μm. **(B)** Quantification of $Ca_V1.4$ and RIBEYE colocalization in WT (blue) and TPBG-KO (KO; orange) using M1 and M2 Mander's coefficients in control (WT: $n$ = 134 puncta; KO: $n$ = 327 puncta) and RBC axon terminals (WT: $n$ = 100 puncta; KO: $n$ = 119 puncta). **(C)** Quantification of RIBEYE puncta counts in WT (blue; $n$ = 90 terminals) and TPBG-KO (KO; orange; $n$ = 109 terminals). Ribeye labeling was quantified as puncta per PKCα-positive area ($um^2$). **(D)** Example FIB-SEM images showing RBC active zones from WT (top) and TPBG-KO (KO; bottom) RBC axon terminals. Scale bar is 500 nm. **(E)** Quantification of synaptic ribbon length in WT (blue; $n$ = 33 ribbons from 9 axon terminals) and TPBG-KO (KO; orange; $n$ = 38 ribbons from 6 axon terminals) measured from the membrane. Box plots extend from the first to the third quartile and the whiskers extend across all points. The line in the box represents the median. ns: $p > 0.05$; ***$p < 0.001$. Please refer to **Supplementary Figure 2** for zoomed-out electron micrographs.

fF; 400 Hz: 19.13 ± 4.06 fF; 800 Hz: 4.05 ± 2.91 fF; 1,600 Hz: −4.23 ± 1.40; Brown-Forsythe ANOVA: $p < 0.0001$, 34.12 (2.00, 10.87)] and the resting $C_m$ [**Supplementary Figures 3E, F**; 200 Hz: 5.97 ± 0.23 pF, 400 Hz: 5.73 ± 0.12 pF, 800 Hz: 4.81 ± 0.15 pF, 1,600 Hz: 4.04 ± 0.12 pF; Brown-Forsythe ANOVA: $p < 0.0001$, 25.06 (3.00, 11.34)] were greater at 200 Hz compared to higher frequencies. These supplementary results support our decision to examine exocytosis in RBCs using a 200 Hz "sine + DC" protocol.

To examine RBC synaptic vesicle exocytosis, we used whole-cell voltage-clamp to compare WT (blue; $n$ = 6) and TPBG-KO (KO; orange; $n$ = 7) voltage-gated $Ca^{2+}$ currents and subsequent changes in membrane capacitance (**Figure 5**). Cells where $C_m$, $R_m$, and $R_s$ were highly correlated were discarded. The synaptic blockers L-AP4, strychnine, TPMPA, and gabazine were used to block spontaneous activity and help increase and stabilize $R_m$ during recordings. The passive properties of $R_m$ [WT: 1.603 ± 0.24 GΩ; KO: 1.630 ± 0.16 GΩ; Welch's $t$-test: $p = 0.93$, $t(8.84) = 0.097$]

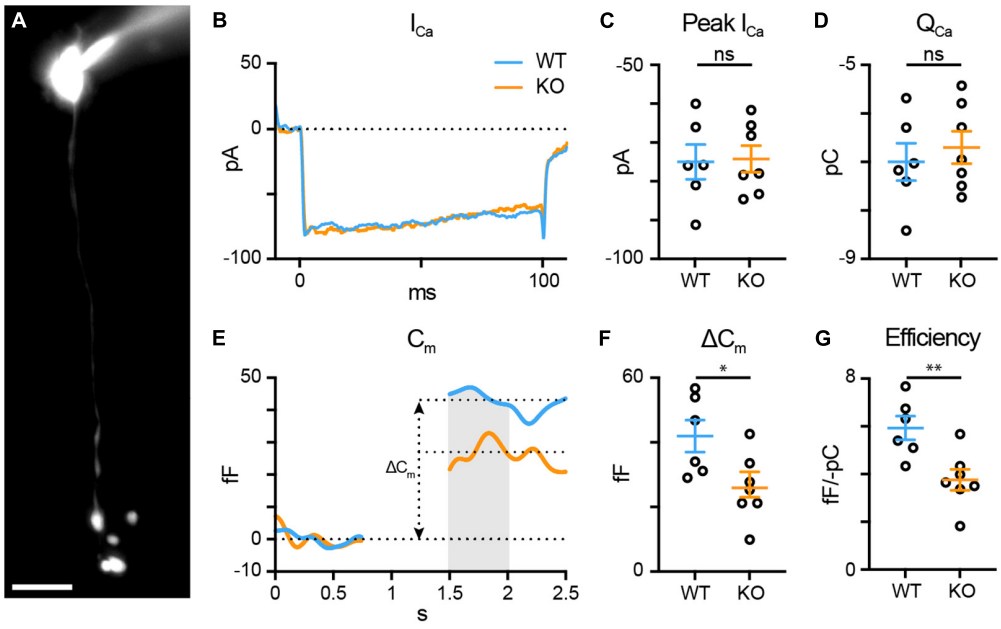


FIGURE 5
TPBG is required for efficient synaptic vesicle release in RBC axon terminals. Whole-cell voltage-clamp recordings were performed in WT (blue; $n$ = 6) and TPBG-KO (KO; orange; $n$ = 7) RBCs. **(A)** Epifluorescence micrograph of an RBC filled with Alexa Fluor 594 Hydrazide after patch-clamp recording. RBCs were patched and cell type was verified *post hoc* using epifluorescence microscopy. The scale bar is 10 μm. **(B)** Average voltage-gated $Ca^{2+}$ current traces recorded after a depolarizing pulse from −80 mV to −10 mV for 100 ms. **(C)** Quantification of peak voltage-gated $Ca^{2+}$ current amplitudes ($I_{Ca}$) and **(D)** charge transfer ($Q_{Ca}$) over the duration of the pulse. **(E)** Average membrane capacitance ($C_m$) recordings using a 200 Hz sine + DC protocol. $\Delta C_m$ was measured as the difference between baselined resting $C_m$ before and after the depolarizing pulse. Data immediately after the pulse was excluded until $C_m$ stabilized. The gray bar represents the region across which $C_m$ values were averaged. **(F)** Quantification of $\Delta C_m$. **(G)** Quantification of exocytosis efficiency calculated as the absolute value of the change in $C_m$ per unit $Q_{Ca}$. Ames medium was supplemented with 1 mM $CaCl_2$ and (in μM): 0.5 strychnine, 3 gabazine, 50 TPMPA, and 4 L-AP4. Open circles in bar graphs represent single cells and bars represent the mean ± SEM. Statistical significance was determined using Welch's $t$-tests; ns: $p > 0.05$; *$p < 0.05$; **$p < 0.01$.

and $R_s$ [WT: 50.54 ± 2.33 MΩ; KO: 49.61 ± 1.91 MΩ; Welch's $t$-test: $p$ = 0.76, $t(10.16)$ = 0.31] were not different between WT and TPBG-KO RBCs. As long as $R_m$ is significantly greater than $R_s$, $\Delta C_m$ should be a faithful approximation of overall exocytosis (Gillis, 2000).

TPBG-KO had no effect on the voltage-gated $Ca^{2+}$ currents [Figures 5B, C; WT: −74.99 ± 4.49 pA, KO: −74.24 ± 3.41 pA; Welch's $t$-test: $p$ = 0.90, $t(9.73)$ = 0.13] or charge transfer [Figure 5D; WT: −7.0 ± 0.38 pC, KO: −6.7 ± 0.33 pC; Welch's $t$-test: $p$ = 0.57, $t(10.43)$ = 0.58]. However, TPBG-KO resulted in a reduction in $\Delta C_m$ compared to WT [Figures 5E, F; WT: 41.94 ± 4.95 fF, KO: 25.90 ± 3.91 fF; Welch's $t$-test: $p$ = 0.029, $t(9.95)$ = 2.55], suggesting a decrease in synaptic vesicle exocytosis in the KO. Most interestingly, the efficiency of exocytosis (the ratio of $\Delta C_m$ per unit $Q_{Ca}$) is also reduced in the KO [Figure 5G; WT: 5.93 ± 0.50 fF/-pC, KO: 3.76 ± 0.44 fF/-pC; Welch's $t$-test: $p$ = 0.0077, $t(10.52)$ = 3.28], indicating that TPBG-KO alters the efficiency of RBC vesicle exocytosis without changing $Ca^{2+}$ influx.

## TPBG does not alter RBC input resistance or excitability

Trophoblast glycoprotein knockout amplifies the RBC light response and reduces synaptic vesicle exocytosis, suggesting that TPBG-KO may reduce the gain of RBC synaptic release by shifting RBC excitability. To compare the excitability between WT (blue; $n$ = 9) and TPBG-KO (KO; orange; $n$ = 11) RBCs, we used current injections (from −80 to 80 pA in 20 pA intervals) in whole-cell current-clamp mode to construct voltage-current relationships and calculate the peak and sustained input resistances ($R_{in}$). For these experiments, we used the synaptic blockers L-AP4, strychnine, TPMPA, and gabazine to isolate RBC-specific voltage responses. Figure 6A shows voltage responses after representative current injections of −80 pA, 0 pA, and + 80 pA. The resting membrane potential ($V_m$) was unchanged in the KO [Figure 6B; WT: −58.02 ± 4.91 mV, KO: −56.35 ± 4.66 mV; Welch's $t$-test: $p$ = 0.81, $t(17.53)$ = 0.25]. We found no difference in peak [Figures 6C, D; WT: 1.40 ± 0.13 GΩ, KO: 1.39 ± 0.09 GΩ; Welch's $t$-test: $p$ = 0.97, $t(14.94)$ = 0.04] or sustained $R_{in}$ [Figures 6E, F; WT: 1.13 ± 0.11 GΩ, KO: 1.05 ± 0.07 GΩ; Welch's $t$-test: $p$ = 0.58, $t(14.28)$ = 0.56] between the WT and KO RBCs. These results indicate that a shift in $R_{in}$ and RBC excitability in the TPBG-KO do not explain the reduced exocytosis.

## TPBG-KO reduces reciprocal inhibitory feedback

Rod bipolar cells drive retinal output via glutamate release into the IPL, which stimulates $Ca^{2+}$-permeable AMPA receptors in

10.3389/fncel.2023.1306006

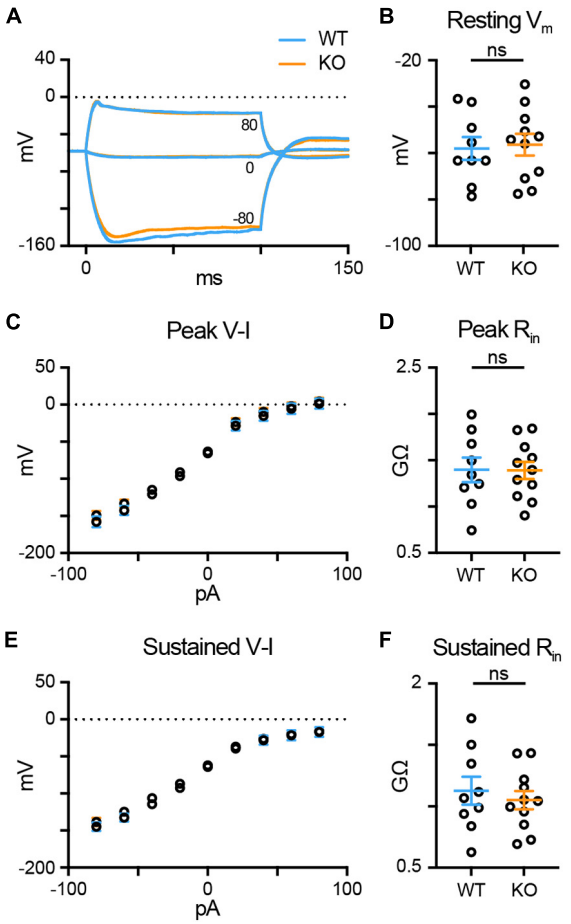


FIGURE 6
TPBG does not alter RBC input resistance or excitability. Whole-cell current-clamp recordings in WT (blue; $n$ = 9) and TPBG-KO (KO; orange; $n$ = 11) RBCs were used to construct a current-voltage relationship and calculate input resistance ($R_{in}$). A current injection protocol from −80 pA to 80 pA in 20 pA steps was used with a K-gluconate-based internal solution. **(A)** Average voltage traces following −80 pA, 0 pA, and 80 pA current injections for 100 ms. **(B)** Resting membrane voltages recorded immediately after entering current clamp mode. **(C)** A plot of the voltage-current (V-I) relationship measured at the peak voltage during current injections. **(D)** Quantification of peak $R_{in}$. **(E)** A plot of the sustained V-I relationship measured as the average voltage calculated over the last 10 ms of the current pulse. **(F)** Quantification of the sustained $R_{in}$. Peak and sustained $R_{in}$ values were calculated by measuring the slope of the linear portion of the V-I curves (from −40 to 40 pA). Ames medium was supplemented with 1 mM $CaCl_2$ and (in μM): 0.5 strychnine, 3 gabazine, 50 TPMPA, and 4 L-AP4. For V-I curves, open circles represent the mean and error bars represent SEM. For quantification, open circles represent single cells and bars represent the mean ± SEM. Statistical significance was determined using Welch's $t$-tests; ns: $p > 0.05$.

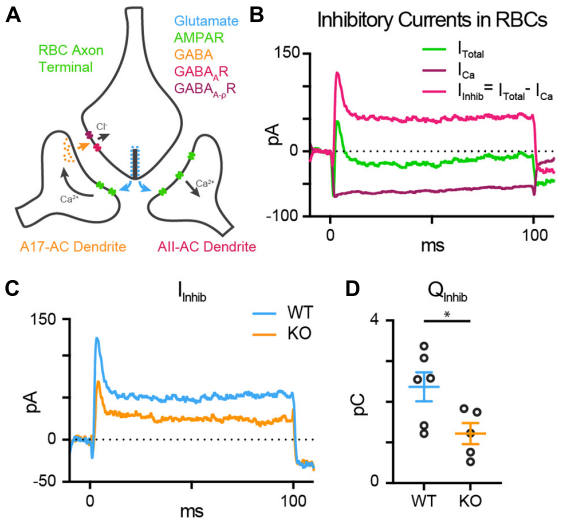


FIGURE 7
TPBG-KO reduces reciprocal inhibitory feedback. **(A)** The dyad synapse arrangement between one RBC, one AII-AC, and one A17-AC in the IPL. Glutamate release by RBCs is detected by $Ca^{2+}$-permeable AMPA receptors (AMPARs) in AII-AC and A17-AC dendrites. A17-ACs then release GABA back onto the synaptic cleft which is sensed by $GABA_A$ receptors ($GABA_AR$s) and $GABA_A\rho$ receptors ($GABA_A\rho$Rs) in the RBC axon terminals. **(B)** Inhibitory currents are superimposed over voltage-gated $Ca^{2+}$ currents. Reciprocal feedback in RBCs was evoked with a 100 ms depolarizing pulse from −80 mV to −10 mV. In the absence of GABA receptor blockers, this depolarizing pulse elicits an inward voltage-gated $Ca^{2+}$ current that is quickly subsumed by outward inhibitory currents ($I_{Total}$; green). These outward currents are abolished by the application of the GABA receptor blockers gabazine and TPMPA ($I_{Ca}$; magenta). Inhibitory currents ($I_{Inhib}$; magenta) can be isolated by subtracting $I_{Ca}$ (maroon) from $I_{Total}$ (green). **(C)** Average whole-cell patch-clamp recordings from WT (blue; $n$ = 6) and TPBG-KO (KO; orange; $n$ = 5) RBCs to compare reciprocal inhibitory feedback ($I_{Inhib} = I_{Total} - I_{Ca}$) after a depolarizing pulse from −80 mV to −10 mV for 100 ms. **(D)** Quantification of the charge transfer ($Q_{Inhib}$) measured from baseline over the duration of the 100 ms stimulus. Ames medium was supplemented with 1 mM $CaCl_2$, 0.5 μM strychnine and 4 μM L-AP4. Open circles in bar graphs represent single cells and bars represent the mean ± SEM. Statistical significance was determined using Welch's $t$-tests; $^*p < 0.05$.

downstream AII amacrine cells (AII-ACs). RBC glutamate release is also detected by A17 amacrine cells (A17-ACs), which when depolarized, release GABA back onto RBC synaptic terminals where it is sensed by $GABA_A$ and $GABA_A\rho$ (also called $GABA_C$) $Cl^-$ channels (Figure 7A). An influx of $Cl^-$ into the axon terminal through open GABA channels provides inhibitory feedback by hyperpolarizing the RBC and shaping further RBC glutamate release (Hartveit, 1996, 1999; Euler and Masland, 2000; Singer and Diamond, 2003; Chávez et al., 2006, 2010). Each RBC active zone forms a dyad synapse with one AII-AC and one A17-AC (Famiglietti and Kolb, 1975; McGuire et al., 1984; Raviola and Dacheux, 1987; Grimes et al., 2010). As A17-mediated reciprocal feedback is driven by RBC glutamate release, the inhibitory feedback currents in the RBCs are an indirect measure of glutamate release from RBCs and would be expected to be reduced concomitantly with reduced RBC exocytosis in the TPBG-KO.

To test the hypothesis that reduced RBC glutamate release results in smaller inhibitory feedback currents in the TPBG-KO, we used whole-cell voltage-clamp to examine the reciprocal inhibitory response to a depolarizing pulse from −80 mV to −10 mV for 100 ms in WT (blue; $n$ = 6) and TPBG-KO (KO; orange; $n$ = 5) RBCs. L-AP4 was used to block spontaneous excitatory inputs and strychnine was used to block glycinergic inhibition. In the absence of GABA receptor blockers, outward currents can be seen superimposed on the evoked voltage-gated $Ca^{2+}$ current (Figure 7B; Green; $I_{Total}$). Inhibitory currents (magenta; $I_{Inhib}$) can be isolated by subtracting voltage-gated $Ca^{2+}$ currents

(maroon; $I_{Ca}$) from the total current. Inhibitory currents (Figure 7C) and the charge transfer across the duration of the stimulus was reduced in the TPBG-KO compared to WT [Figure 7D; WT: 2.35 ± 0.37 pC; KO: 1.13 ± 0.22 pC; Welch's *t*-test: $p = 0.022$, $t(7.83) = 2.83$]. This supports our previous result that the TPBG-KO suppresses RBC vesicle exocytosis and glutamate release (see Figure 5F).

It is possible that reciprocal feedback is altered in TPBG-KO due to disrupted expression or clustering of GABA receptors in RBC axon terminals. RBCs express both $GABA_A\alpha1$ and $GABA_A\rho1$ receptor subunits in their axon terminals (Fletcher et al., 1998; Palmer, 2006). To see whether TPBG-KO alters GABA receptor expression patterns, we used double immunofluorescence labeling of WT and TPBG-KO whole mount retinas using an antibody against PKCα and antibodies against $GABA_A\alpha1$ (WT: $n = 18$ terminals; KO $n = 28$ terminals) and $GABA_A\rho1$ (WT: $n = 20$ terminals; KO $n = 27$ terminals) receptor subunits (Figure 8). As previously, we isolated RBC axon terminal-specific labeling using a binary mask derived from PKCα immunofluorescence. Next, we counted the GABA puncta per unit area in PKCα-positive axon terminals. We did not observe any major differences in puncta/$\mu m^2$ between WT and TPBG-KO (KO) retinas labeled against either $GABA_A\alpha1$ [Figures 8A, B; WT: 1.21 ± 0.05 puncta/$\mu m^2$; KO: 1.40 ± 0.09 puncta/$\mu m^2$; Welch's *t*-test: $p = 0.064$, $t(39.73) = 1.91$] or $GABA_A\rho1$ [Figures 8C, D; WT: 1.03 ± 0.03 puncta/$\mu m^2$; KO: 0.98 ± 0.03 puncta/$\mu m^2$; Welch's *t*-test: $p = 0.20$, $t(41.11) = 1.29$], indicating that impaired GABA receptor expression is likely not reducing inhibitory feedback. Taken together, our data supports the conclusion that TPBG is required for normal synaptic ribbon development and efficient glutamate release from RBC axon terminals.

# Discussion

In this study, we characterized the functional consequences of genetic knockout of TPBG in the mouse retina using immunofluorescence and electrophysiological approaches. TPBG-KO did not alter gross RBC morphology in the OPL or IPL as PKCα-labeled RBC dendrites and axon terminals appear normal in both conditions. Because TPBG is localized to both the dendrites and axon terminals of RBCs (Wakeham et al., 2020), we sought to examine the effect of TPBG-KO on the RBC synaptic structure and physiology in both compartments. Though ERG b-waves were larger in the TPBG-KO, dendritic TRPM1 currents activated by CPPG (simulated light responses) did not change; however, we cannot rule out an effect on true light responses. In contrast to the larger b-waves, the scotopic OPs were smaller in the KO, suggesting changes in RBC ribbon synapse function. Accordingly, time-resolved $C_m$ measurements and whole-cell recording indicated that synaptic vesicle exocytosis and GABAergic feedback are reduced at TPBG-KO RBC synapses, and synaptic ribbons are shorter. Importantly, we did not detect differences in presynaptic voltage-gated $Ca^{2+}$ current amplitude or changes in $Ca^{2+}$ channel, GABA receptor, or RIBEYE expression and localization. We propose that TPBG plays an important role in fine tuning the synaptic architecture of RBC ribbon synapses to increase exocytosis efficiency.

## TPBG and RBC synaptic vesicle exocytosis

We found a reduction in the OPs isolated from scotopic ERG recordings in TPBG-KO mice, which we interpret as evidence for decreased RBC output to third-order neurons. While we cannot rule out a contribution of the TPBG-expressing amacrine cells to the reduced OP amplitudes in the TPBG-KO, the similarity of the OP phenotype to that seen in the PKCα-KO (Xiong et al., 2015) suggests that it is due to an RBC defect. Furthermore, pharmacological dissection of ERG components points to the RBC to AII/A17 reciprocal synapse as the origin of the OPs (Wachtmeister, 1998; Liao et al., 2023). Early studies implicated interactions between bipolar cell axon terminals, amacrine cell processes, and ganglion cell dendrites as potential generators of the OPs (Ogden, 1973). Intravitreal injections of glycine into rabbit retinas resulted in morphological changes in many ACs and disappearance of the OPs from the ERG (Korol et al., 1975) while application of neurotoxic kainate to ganglion cell dendrites diminishes OP amplitude (Vaegan and Millar, 1994). A more recent study unequivocally implicates multiple distinct generators in the production of early, intermediate, and late OP peaks (Dong et al., 2004). The use of APB and CNQX to block synaptic inputs to ON and OFF-bipolar cells significantly diminished intermediate and later OPs but left early OPs intact, suggesting that early OPs are generated by photoreceptors. Intermediate and late OPs have differential sensitivity to tetrodotoxin, which abolished only late OPs, indicating that intermediate OPs are generated by action-potential-independent interactions and late OPs are generated by action-potential-dependent ones (Dong et al., 2004). Thus, the results of these studies support our conclusion that reduced scotopic OPs are likely due to suppressed rhythmic activity of third-order neurons due to reduced RBC glutamate release.

The $Ca^{2+}$ current amplitudes we recorded (−75 pA) following a depolarizing step are significantly larger than those previously reported [−30 pA by Protti and Llano (1998) and −20 pA by Singer and Diamond (2003)]. We also recorded larger $C_m$ jumps (42 fF in WT) than those reported from dissociated RBCs [30 fF in Zhou et al. (2006)]. We believe these differences can be attributed to higher recording temperatures (33°C vs. 21°C) and our use of older animals. With a mean resting $C_m$ of 5.97 pF and a mean $R_s$ of 50.04 MΩ, we can calculate an average voltage-clamp speed of 298.74 μs – sufficiently fast to clamp the membrane to a 200 Hz sine wave with a 5 ms period.

Exocytosis efficiency is calculated as the exocytosis per unit $Ca^{2+}$ charge transfer. We calculated an exocytosis efficiency of approximately 6 fF/pC in adult WT mouse RBCs after a 100 ms depolarizing pulse at 33°C. In adult vertebrate auditory hair cells, which also form ribbon synapses, similar exocytosis efficiencies of 5 to 6 fF/pC have been reported after 100 ms pulses (Chen and von Gersdorff, 2019; Moser et al., 2020). Rod bipolar cell ribbon synapses operate via nanodomain coupling between $Ca^{2+}$ channels and docked vesicles (Jarsky et al., 2010), whereas immature calyx of Held synapses contain conventional active zones that operate via $Ca^{2+}$ microdomains where $Ca^{2+}$ influx triggers vesicle exocytosis from greater distances (Kushmerick et al., 2006). Further studies will be required to verify the relationship between TPBG and nanodomain coupling at RBC ribbon synapses.

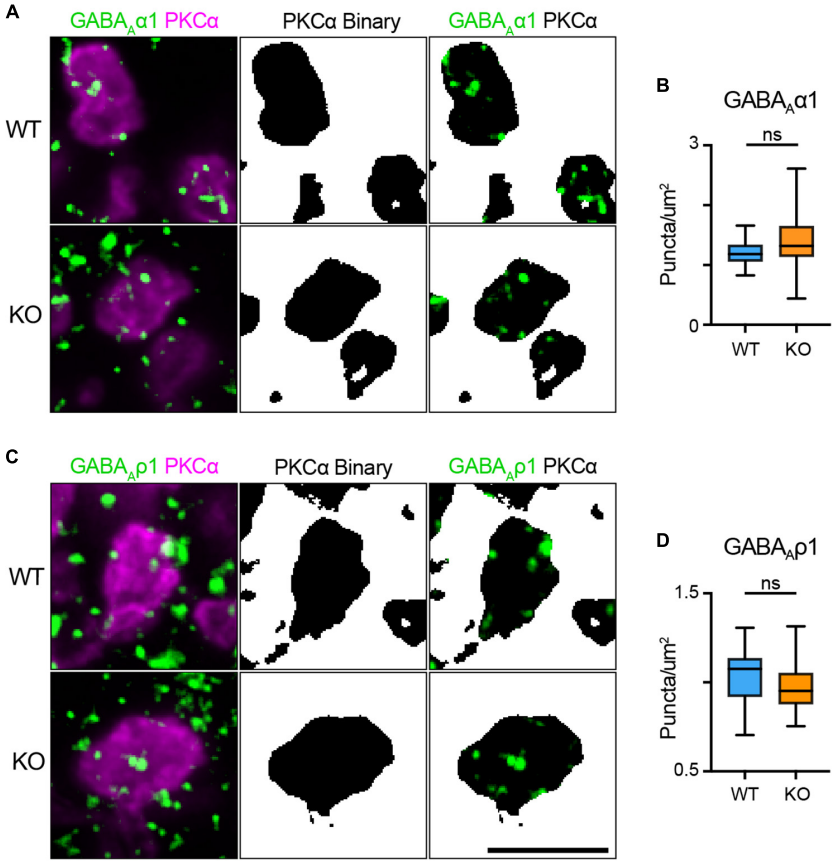


FIGURE 8
TPBG is not required for localization of GABA receptor immunofluorescence to RBC axon terminals. Immunofluorescence confocal microscopy of WT and TPBG-KO (KO) whole mount retinas using an antibody against PKCα (magenta) and antibodies against either the GABA$_A$α1 subunit [**(A)**; green; WT: $n$ = 18 terminals; KO $n$ = 28 terminals] or the GABA$_A$ρ1 subunit [**(C)**; green; WT: $n$ = 20 terminals; KO $n$ = 27 terminals]. To isolate labeling in RBC axon terminals, binaries were created using the PKCα channel and overlayed over the other channels to generate binary masks. For all images, Z-projections of two sections were used with a Z-step distance of 0.297 μm for a total thickness of 0.547 μm. Scale bar is 5 μm. **(B)** Quantification of GABA$_A$α1 subunit puncta/μm$^2$. **(D)** Quantification of GABA$_A$α1 subunit puncta/μm$^2$. Box plots extend from the first to the third quartile and the whiskers extend across all points. The line in the box represents the median. Statistical significance was determined using Welch's $t$-tests; ns: $p > 0.05$.

## TPBG and synaptic ribbon proteins

Synaptic docking, $Ca^{2+}$ influx and its detection by $Ca^{2+}$ sensors, and $Ca^{2+}$-dependent fusion of synaptic vesicles with the presynaptic membrane are all potential points at which TPBG may be supporting efficient vesicle release from RBCs. Vesicle accumulation and transport in RBC synaptic terminals is dependent on F-actin polymerization and is regulated by PKCα (Job and Lagnado, 1998; Minami et al., 1998; Tachibana, 1999; Doussau and Augustine, 2000; Berglund et al., 2002). We originally identified TPBG as a PKCα-dependent phosphoprotein (Wakeham et al., 2019); thus, it is possible that PKCα controls vesicle docking via actin dynamics in RBC axon terminals through TPBG.

The tight temporal control of vesicle release that is a trademark of synaptic ribbons requires nanodomain-coupling between L-type voltage-gated $Ca^{2+}$ channels and $Ca^{2+}$ binding proteins that trigger synaptic vesicle fusion (Jarsky et al., 2010; Eggermann et al., 2012; Balakrishnan et al., 2015). Synaptic ribbons are primarily composed of the scaffold protein RIBEYE and are anchored to the presynaptic active zone by a number of cytoskeletal anchoring proteins, including Bassoon and Piccolo (Zanazzi and Matthews, 2009). We did not observe a difference in RIBEYE immunofluorescence in WT and TPBG-KO axon terminals and electron microscopy showed normal positioning of ribbons at RBC active zones in the KO. $Ca_V1.4$ and RIBEYE appear co-localized by immunofluorescence in both WT and TPBG-KO RBC axon terminals, but a small disruption of this tight coupling might not be detected with immunofluorescence and could have a large effect on glutamate release by slowing the accumulation of $Ca^{2+}$ at the sensor. It is possible that TPBG facilitates $Ca^{2+}$ channel clustering or association between the channels and the ribbon such that, in its absence, normal nanodomain coupling is disrupted and synaptic vesicle fusion is reduced.

Ultrastructural analysis of RBC axon terminals revealed that the synaptic ribbons are approximately 15% smaller in TPBG-KO RBCs compared to WT. Shorter ribbons could result in a smaller number of ribbon-attached vesicles that may constitute a smaller ready releasable pool (RRP), resulting in the observed $C_m$ jump attenuation. The density of ribbons was not reduced in the TPBG-KO as assayed by immunofluorescence imaging, nor were $Ca^{2+}$

currents changed; thus, the smaller $C_m$ jumps could not be due to a smaller number of ribbons or reduced $Ca^{2+}$ influx. We used a large 100 ms depolarizing pulse to evoke vesicle release which likely exhausts the fast RRP and potentially depletes the secondary RRP. The fast RRP probably consists of the first row of vesicles lining the bottom of the ribbon closest to the active zone (von Gersdorff et al., 1996; von Gersdorff and Matthews, 1997) and this pool may not be affected by a shorter ribbon. In contrast, a shorter ribbon may significantly reduce the size of the secondary RRP, presumably corresponding to vesicles tethered higher on the ribbon, leading to reduced $C_m$ jumps. Indeed, in RIBEYE-KO mice, where the synaptic ribbon is absent, exocytosis is greatly reduced in RBC and rod photoreceptor synapses (Maxeiner et al., 2016; Grabner and Moser, 2021). More experimentation is required to determine exactly how the shorter ribbons in the TPBG-KO RBC axon terminals affects the different vesicle pools.

## TPBG and reciprocal feedback inhibition

To confirm that the TPBG-KO reduces RBC vesicle fusion and glutamate release, we compared GABAergic feedback inhibition between WT and TPBG-KO RBCs. We found attenuation of inhibitory charge transfer in the TPBG-KO without a change in GABA receptor expression or localization. With glycinergic inhibition blocked by strychnine, the primary remaining source of feedback inhibition in RBCs is A17-mediated GABAergic reciprocal feedback (Grimes et al., 2015). We note that our peak WT GABA receptor currents of ~125 pA and sustained currents of ~50 pA are considerably larger than reported previously in mouse RBCs (Chávez et al., 2010). Again, we attribute this to our use of older animals and higher recording temperatures and, perhaps, to the use of Ames recording solutions instead of artificial CSF: Ames contains ascorbic acid, an enhancer of GABA currents (Calero et al., 2011) that was not included in previous studies of reciprocal GABAergic feedback currents (Chávez et al., 2010).

Trophoblast glycoprotein knockout increased scotopic ERG b-waves, suggesting an increase in RBC depolarization. The scotopic ERG b-wave is initiated by current through TRPM1 non-specific cation channels in the RBC dendrites. Yet, we did not find any difference in CPPG-induced TRPM1 currents between WT and TPBG-KO retinas and the input resistance and excitability of the RBC was unchanged. However, the scotopic b-wave is also shaped by reciprocal inhibition. Pharmacological studies show that blocking inhibitory currents from third-order neurons changes the scotopic b-wave. In particular, injections of a $GABA_A$ antagonist (bicuculline) or a $GABA_A\rho$ antagonist (TPMPA) into the IPL significantly increases the amplitude and duration of the scotopic b-wave (Dong and Hare, 2000, 2003), suggesting that GABAergic feedback from A17-ACs contributes to the shape of the RBC light response. We suggest that the enlarged ERG b-wave in the TPBG-KO is due to reduced inhibitory feedback onto the RBC terminals, secondary to reduced RBC glutamate release by the RBC.

## Summary

Our findings show that genetic deletion of TPBG attenuates scotopic ERG oscillatory potentials, synaptic vesicle exocytosis from RBCs, and reciprocal feedback onto RBCs. We propose that TPBG is required for efficient coupling of $Ca^{2+}$ influx and glutamate release at RBC active zones, possibly through its effect on synaptic ribbons. Further evaluation of TPBG is critical for producing a more comprehensive understanding of its role in fine-tuning RBC synaptic ribbon physiology.

## Significance statement

Retinal rod bipolar cells (RBCs) must reliably detect and transform visual signals over a wide range of luminance and contrast conditions. To achieve this, the presynaptic active zones RBCs contain specialized synaptic ribbons that cluster synaptic vesicles near the presynaptic membrane and promote extremely precise, rapid, and sustained neurotransmitter release in response to graded changes in membrane potential. Here we show that knockout of the leucine-rich repeat protein trophoblast glycoprotein (TPBG) reduces synaptic ribbon length and attenuates synaptic vesicle exocytosis from RBC axon terminals. Therefore, we propose that TPBG is required for synaptic ribbon development and efficient synaptic vesicle exocytosis at RBC synapses.

## Data availability statement

The raw data supporting the conclusions of this article will be made available by the authors, without undue reservation.

## Ethics statement

The animal study was approved by the OHSU Institutional Animal Care and Use Committee. The study was conducted in accordance with the local legislation and institutional requirements.

## Author contributions

CW: Conceptualization, Data curation, Formal analysis, Investigation, Writing—original draft. QS: Formal analysis, Writing—review and editing, Investigation. GR: Investigation, Writing—review and editing. TH: Investigation, Writing—review and editing. RD: Investigation, Writing—review and editing, Conceptualization. HvG: Conceptualization, Writing—review and editing, Supervision, Resources. CM: Conceptualization, Supervision, Writing—review and editing, Formal analysis, Funding acquisition, Resources.

## Funding

The author(s) declare financial support was received for the research, authorship, and/or publication of this article. This work

was supported by NIH grants to CM (R01 EY029985 and P30 EY010572) and HvG (R01 EY014043, R01 DC012938, and R01 EY032564).

## Acknowledgments

We would like to thank R. Lane Brown, Marc A. Meadows, and André A. Dagostin for assistance with patch clamp electrophysiology and data analysis. We would also like to thank the OHSU Neuroscience Imaging Center's Ultrastructure and Single Particle Microscopy Core (P30 NS061800) for FIB-SEM data collection.

## Conflict of interest

The authors declare that the research was conducted in the absence of any commercial or financial relationships that could be construed as a potential conflict of interest.

## Publisher's note

All claims expressed in this article are solely those of the authors and do not necessarily represent those of their affiliated organizations, or those of the publisher, the editors and the reviewers. Any product that may be evaluated in this article, or claim that may be made by its manufacturer, is not guaranteed or endorsed by the publisher.

## Supplementary material

The Supplementary Material for this article can be found online at: https://www.frontiersin.org/articles/10.3389/fncel.2023.1306006/full#supplementary-material

SUPPLEMENTARY FIGURE 1
TPBG-KO does not alter the scotopic ERG a-wave. Quantification of a-wave amplitudes recorded after light stimuli [−0.06 to 1.93 log(cd·s/$m^2$)]. A-waves are measured from baseline to the a-wave trough. Data is presented as the mean ± SEM.

SUPPLEMENTARY FIGURE 2
FIB-SEM imaging of RBC axon terminals. Focused ion beam scanning electron microscopy (FIB-SEM) was used to image RBC axon terminals in the distal IPL and examine synaptic ribbon location and morphology. Zoomed-out examples of WT and TPBG-KO (KO) RBC axon terminals in the IPL. The scale bar is 5 μ m.

SUPPLEMENTARY FIGURE 3
Measuring membrane capacitance in RBCs. **(A)** Whole-cell voltage-clamp capacitance recordings were made using the "sine + DC" method. A sinusoidal voltage command (200 Hz at 30 mV trough-to-peak) was superimposed on the holding potential of −80 mV. Membrane capacitance ($C_m$), membrane resistance ($R_m$), and series resistance ($R_s$) were recorded before and after a depolarizing pulse from −80 mV to −10 mV for 100 ms. **(B)** A sample recording from a WT RBC using the sine + DC method as described. The change in membrane capacitance ($\Delta C_m$) was measured as the difference between the $C_m$ before and after the depolarizing pulse. Changes to $R_m$ (middle) and $R_s$ (bottom) were small and do not correlate with changes in $C_m$. **(C)** Average baseline-subtracted $C_m$ recordings using 200 Hz (blue; $n$ = 6), 400 Hz (orange; $n$ = 4), 800 Hz (green; $n$ = 4), or 1,600 Hz (magenta; $n$ = 4) sinusoidal voltage commands in WT RBCs. Data for the 200 Hz condition was reused from WT in **Figure 4**. Traces with higher frequencies were resampled to 200 Hz for ease of comparisons. **(D)** Quantification of $\Delta C_m$. **(E)** Average $C_m$ recordings and **(F)** quantification of resting $C_m$ across frequencies. Resting $C_m$ was measured before the depolarizing pulse. Open circles in bar graphs represent single cells and bars represent the mean ± SEM. Statistical significance was determined using Brown-Forsythe ANOVA tests; $^{****}p < 0.0001$.

## References

Agosto, M. A., and Wensel, T. G. (2020). LRRTM4 is a member of the transsynaptic complex between rod photoreceptors and bipolar cells. *J. Comp. Neurol.* 529, 221–233. doi: 10.1002/cne.24944

Ames, A., and Nesbett, F. B. (1981). In vitro retina as an experimental model of the central nervous system. *J. Neurochem.* 37, 867–877. doi: 10.1111/j.1471-4159.1981.tb04473.x

Balakrishnan, V., Puthussery, T., Kim, M.-H., Taylor, W. R., and von Gersdorff, H. (2015). Synaptic vesicle exocytosis at the dendritic lobules of an inhibitory interneuron in the mammalian retina. *Neuron* 87, 563–575. doi: 10.1016/j.neuron.2015.07.016

Berglund, K., Midorikawa, M., and Tachibana, M. (2002). Increase in the pool size of releasable synaptic vesicles by the activation of protein kinase c in goldfish retinal bipolar cells. *J. Neurosci.* 22, 4776–4785. doi: 10.1523/jneurosci.22-12-04776.2002

Calero, C. I., Vickers, E., Cid, G. M., Aguayo, L. G., von Gersdorff, H., and Calvo, D. J. (2011). Allosteric modulation of retinal GABA receptors by ascorbic acid. *J. Neurosci.* 31, 9672–9682. doi: 10.1523/jneurosci.5157-10.2011

Cao, Y., Posokhova, E., and Martemyanov, K. A. (2011). TRPM1 forms complexes with nyctalopin in vivo and accumulates in postsynaptic compartment of on-bipolar neurons in mglur6-dependent manner. *J. Neurosci.* 31, 11521–11526. doi: 10.1523/jneurosci.1682-11.2011

Cao, Y., Sarria, I., Fehlhaber, K. E., Kamasawa, N., Orlandi, C., James, K. N., et al. (2015). Mechanism for selective synaptic wiring of rod photoreceptors into the retinal circuitry and its role in vision. *Neuron* 87, 1248–1260. doi: 10.1016/j.neuron.2015.09.002

Cao, Y., Wang, Y., Dunn, H. A., Orlandi, C., Shultz, N., Kamasawa, N., et al. (2020). Interplay between cell-adhesion molecules governs synaptic wiring of cone photoreceptors. *Proc. Natl. Acad. Sci. U.S.A.* 117, 23914–23924. doi: 10.1073/pnas.2009940117

Chávez, A. E., Grimes, W. N., and Diamond, J. S. (2010). Mechanisms underlying lateral GABAergic feedback onto rod bipolar cells in rat retina. *J. Neurosci.* 30, 2330–2339. doi: 10.1523/jneurosci.5574-09.2010

Chávez, A. E., Singer, J. H., and Diamond, J. S. (2006). Fast neurotransmitter release triggered by Ca influx through AMPA-type glutamate receptors. *Nature* 443, 705–708. doi: 10.1038/nature05123

Chen, M., and von Gersdorff, H. (2019). How to build a fast and highly sensitive sound detector that remains robust to temperature shifts. *J. Neurosci.* 39, 7260–7276. doi: 10.1523/jneurosci.2510-18.2019

Dong, C.-J., Agey, P., and Hare, W. A. (2004). Origins of the electroretinogram oscillatory potentials in the rabbit retina. *Visual Neurosci.* 21, 533–543. doi: 10.1017/s0952523804214043

Dong, C.-J., and Hare, W. A. (2000). Contribution to the kinetics and amplitude of the electroretinogram b-wave by third-order retinal neurons in the rabbit retina. *Vision Res.* 40, 579–590. doi: 10.1016/s0042-6989(99)00203-5

Dong, C.-J., and Hare, W. A. (2003). Temporal modulation of scotopic visual signals by A17 amacrine cells in mammalian retina in vivo. *J. Neurophysiol.* 89, 2159–2166. doi: 10.1152/jn.01008.2002

Doussau, F., and Augustine, G. J. (2000). The actin cytoskeleton and neurotransmitter release: An overview. *Biochimie* 82, 353–363. doi: 10.1016/s0300-9084(00)00217-0

Eggermann, E., Bucurenciu, I., Goswami, S. P., and Jonas, P. (2012). Nanodomain coupling between Ca2+ channels and sensors of exocytosis at fast mammalian synapses. *Nat. Rev. Neurosci.* 13, 7–21. doi: 10.1038/nrn3125

Euler, T., and Masland, R. H. (2000). Light-evoked responses of bipolar cells in a mammalian retina. *J. Neurophysiol.* 83, 1817–1829. doi: 10.1152/jn.2000.83.4.1817

Famiglietti, E. V., and Kolb, H. (1975). A bistratified amacrine cell and synaptic cirucitry in the inner plexiform layer of the retina. *Brain Res.* 84, 293–300.

Fletcher, E. L., Koulen, P., and Wässle, H. (1998). GABAA and GABAC receptors on mammalian rod bipolar cells. *J. Comp. Neurol.* 396, 351–365.

Gillis, K. D. (2000). Admittance-based measurement of membrane capacitance using the EPC-9 patch-clamp amplifier. *Pflügers Archiv.* 439, 655–664. doi: 10.1007/s004249900173

Grabner, C. P., and Moser, T. (2021). The mammalian rod synaptic ribbon is essential for Cav channel facilitation and ultrafast synaptic vesicle fusion. *ELife* 10, e63844. doi: 10.7554/elife.63844

Grimes, W. N., Zhang, J., Graydon, C. W., Kachar, B., and Diamond, J. S. (2010). Retinal parallel processors: More than 100 independent microcircuits operate within a single interneuron. *Neuron* 65, 873–885. doi: 10.1016/j.neuron.2010.02.028

Grimes, W. N., Zhang, J., Tian, H., Graydon, C. W., Hoon, M., Rieke, F., et al. (2015). Complex inhibitory microcircuitry regulates retinal signaling near visual threshold. *J. Neurophysiol.* 114, 341–353. doi: 10.1152/jn.00017.2015

Hartveit, E. (1996). Membrane currents evoked by ionotropic glutamate receptor agonists in rod bipolar cells in the rat retinal slice preparation. *J. Neurophysiol.* 76, 401–422. doi: 10.1152/jn.1996.76.1.401

Hartveit, E. (1999). Reciprocal synaptic interactions between rod bipolar cells and amacrine cells in the rat retina. *J. Neurophysiol.* 81, 2923–2936. doi: 10.1152/jn.1999.81.6.2923

Hasan, N., Pangeni, G., Cobb, C. A., Ray, T. A., Nettesheim, E. R., Ertel, K. J., et al. (2019). Presynaptic Expression of LRIT3 Transsynaptically Organizes the Postsynaptic Glutamate Signaling Complex Containing TRPM1. *Cell Rep.* 27, 3107–3116.e1. doi: 10.1016/j.celrep.2019.05.056

Hasan, N., Pangeni, G., Ray, T. A., Fransen, K. M., Noel, J., Borghuis, B. G., et al. (2020). ). LRIT3 is required for Nyctalopin expression and normal ON and OFF pathway signaling in the retina. *ENeuro* 7, ENEURO.0002–ENEURO.20. doi: 10.1523/eneuro.0002-20.2020

Hasan, N., Ray, T. A., and Gregg, R. G. (2016). CACNA1S expression in mouse retina: Novel isoforms and antibody cross-reactivity with GPR179. *Vis. Neurosci.* 33, E009. doi: 10.1017/s0952523816000055

Jarsky, T., Tian, M., and Singer, J. H. (2010). Nanodomain control of exocytosis is responsible for the signaling capability of a retinal ribbon synapse. *J. Neurosci.* 30, 11885–11895. doi: 10.1523/jneurosci.1415-10.2010

Job, C., and Lagnado, L. (1998). Calcium and protein kinase C regulate the actin cytoskeleton in the synaptic terminal of retinal bipolar cells. *J. Cell Biol.* 143, 1661–1672. doi: 10.1083/jcb.143.6.1661

Kim, M.-H., and von Gersdorff, H. (2016). Postsynaptic plasticity triggered by Ca2+-Permeable AMPA receptor activation in retinal amacrine cells. *Neuron* 89, 507–520. doi: 10.1016/j.neuron.2015.12.028

Klyachko, V. A., and Jackson, M. B. (2002). Capacitance steps and fusion pores of small and large-dense-core vesicles in nerve terminals. *Nature* 418, 89–92. doi: 10.1038/nature00852

Kobe, B., and Deisenhofer, J. (1994). The leucine-rich repeat: a versatile binding motif. *Trends Biochem. Sci.* 19, 415–421. doi: 10.1016/0968-0004(94)90090-6

Kobe, B., and Kajava, A. V. (2001). The leucine-rich repeat as a protein recognition motif. *Curr. Opin. Struct. Biol.* 11, 725–732. doi: 10.1016/s0959-440x(01)00266-4

Koike, C., Numata, T., Ueda, H., Mori, Y., and Furukawa, T. (2010a). TRPM1: A vertebrate TRP channel responsible for retinal ON bipolar function. *Cell Calcium* 48, 95–101. doi: 10.1016/j.ceca.2010.08.004

Koike, C., Obara, T., Uriu, Y., Numata, T., Sanuki, R., Miyata, K., et al. (2010b). TRPM1 is a component of the retinal ON bipolar cell transduction channel in the mGluR6 cascade. *Proc. Natl. Acad. Sci. U.S.A.* 107, 332–337. doi: 10.1073/pnas.0912730107

Korol, S., Leuenberger, P. M., Englert, U., and Babel, J. (1975). In vivo effects of glycine on retinal ultrastructure and averaged electroretinogram. *Brain Res.* 97, 235–251. doi: 10.1016/0006-8993(75)90447-3

Kushmerick, C., Renden, R., and von Gersdorff, H. (2006). Physiological temperatures reduce the rate of vesicle pool depletion and short-term depression via an acceleration of vesicle recruitment. *J. Neurosci.* 26, 1366–1377. doi: 10.1523/jneurosci.3889-05.2006

Liao, F., Liu, H., Milla-Navarro, S., Villa, P., and Germain, F. (2023). Origin of retinal oscillatory potentials in the mouse, a tool to specifically locate retinal damage. *Int. J. Mol. Sci.* 24:3126. doi: 10.3390/ijms24043126

Masu, M., Iwakabe, H., Tagawa, Y., Miyoshi, T., Yamashita, M., Fukuda, Y., et al. (1995). Specific deficit of the ON response in visual transmission by targeted disruption of the mGIuR6 gene. *Cell* 80, 757–765. doi: 10.1016/0092-8674(95)90354-2

Maxeiner, S., Luo, F., Tan, A., Schmitz, F., and Südhof, T. C. (2016). How to make a synaptic ribbon: RIBEYE deletion abolishes ribbons in retinal synapses and disrupts neurotransmitter release. *EMBO J.* 35, 1098–1114. doi: 10.15252/embj.201592701

McGuire, B., Stevens, J., and Sterling, P. (1984). Microcircuitry of bipolar cells in cat retina. *J. Neurosci.* 4, 2920–2938. doi: 10.1523/jneurosci.04-12-02920.1984

Minami, N., Berglund, K., Sakaba, T., Kohmoto, H., and Tachibana, M. (1998). Potentiation of transmitter release by protein kinase C in goldfish retinal bipolar cells. *J. Physiol.* 512, 219–225. doi: 10.1111/j.1469-7793.1998.219bf.x

Morgans, C. W. (2000). Neurotransmitter release at ribbon synapses in the retina. *Immunol. Cell Biol.* 78, 442–446. doi: 10.1046/j.1440-1711.2000.00923.x

Morgans, C. W., Zhang, J., Jeffrey, B. G., Nelson, S. M., Burke, N. S., Duvoisin, R. M., et al. (2009). TRPM1 is required for the depolarizing light response in retinal ON-bipolar cells. *Proc. Natl. Acad. Sci. U.S.A.* 106, 19174–19178. doi: 10.1073/pnas.0908711106

Moser, T., Grabner, C. P., and Schmitz, F. (2020). Sensory processing at ribbon synapses in the retina and the cochlea. *Physiol. Rev.* 100, 103–144. doi: 10.1152/physrev.00026.2018

Nakajima, Y., Iwakabe, H., Akazawa, C., Nawa, H., Shigemoto, R., Mizuno, N., et al. (1993). Molecular characterization of a novel retinal metabotropic glutamate receptor mGluR6 with a high agonist selectivity for L-2-amino-4-phosphonobutyrate. *J. Biol. Chem.* 268, 11868–11873.

Neher, E., and Marty, A. (1982). Discrete changes of cell membrane capacitance observed under conditions of enhanced secretion in bovine adrenal chromaffin cells. *Proc. Natl. Acad. Sci. U.S.A.* 79, 6712–6716. doi: 10.1073/pnas.79.21.6712

Neuillé, M., Cao, Y., Caplette, R., Guerrero-Given, D., Thomas, C., Kamasawa, N., et al. (2017). LRIT3 Differentially Affects Connectivity and Synaptic Transmission of Cones to ON- and OFF-Bipolar CellsLRIT3's Role in Cone to Bipolar Cell Transmission. *Investig. Ophthalmol. Vis. Sci.* 58, 1768–1778. doi: 10.1167/iovs.16-20745

Neuillé, M., Morgans, C. W., Cao, Y., Orhan, E., Michiels, C., Sahel, J., et al. (2015). LRIT3 is essential to localize TRPM1 to the dendritic tips of depolarizing bipolar cells and may play a role in cone synapse formation. *Eur. J. Neurosci.e* 42, 1966–1975. doi: 10.1111/ejn.12959

Ogden, T. E. (1973). The oscillatory waves of the primate electroretinogram. *Vis. Res.* 13, 1059–IN4. doi: 10.1016/0042-6989(73)90144-2

Oltedal, L., and Hartveit, E. (2010). Transient release kinetics of rod bipolar cells revealed by capacitance measurement of exocytosis from axon terminals in rat retinal slices. *J. Physiol.* 588, 1469–1487. doi: 10.1113/jphysiol.2010.186916

Oltedal, L., Veruki, M. L., and Hartveit, E. (2009). Passive membrane properties and electrotonic signal processing in retinal rod bipolar cells. *J. Physiol.* 587, 829–849. doi: 10.1113/jphysiol.2008.165415

Palmer, M. J. (2006). Functional segregation of synaptic GABAA and GABAC receptors in goldfish bipolar cell terminals. *J. Physiol.* 577, 45–53. doi: 10.1113/jphysiol.2006.119560

Paridaen, J. T. M. L., Wilsch-Bräuninger, M., and Huttner, W. B. (2013). Asymmetric inheritance of centrosome-associated primary cilium membrane directs ciliogenesis after cell division. *Cell* 155, 333–344. doi: 10.1016/j.cell.2013.08.060

Pearring, J. N., Bojang, P., Shen, Y., Koike, C., Furukawa, T., Nawy, S., et al. (2011). A role for nyctalopin, a small leucine-rich repeat protein, in localizing the TRP melastatin 1 channel to retinal depolarizing bipolar cell dendrites. *J. Neurosci.* 31, 10060–10066. doi: 10.1523/jneurosci.1014-11.2011

Protti, D. A., and Llano, I. (1998). Calcium currents and calcium signaling in rod bipolar cells of Rat Retinal Slices. *J. Neurosci.* 18, 3715–3724. doi: 10.1523/jneurosci.18-10-03715.1998

Raviola, E., and Dacheux, R. F. (1987). Excitatory dyad synapse in rabbit retina. *Proc. Natl. Acad. Sci. U.S.A.* 84, 7324–7328. doi: 10.1073/pnas.84.20.7324

Robson, J. G., and Frishman, L. J. (2014). The rod-driven a-wave of the dark-adapted mammalian electroretinogram. *Prog. Retinal Eye Res.* 39, 1–22. doi: 10.1016/j.preteyeres.2013.12.003

Schindelin, J., Arganda-Carreras, I., Frise, E., Kaynig, V., Longair, M., Pietzsch, T., et al. (2012). Fiji: an open-source platform for biological-image analysis. *Nat. Methods* 9, 676–682. doi: 10.1038/nmeth.2019

Shen, Y., Heimel, J. A., Kamermans, M., Peachey, N. S., Gregg, R. G., and Nawy, S. (2009). A transient receptor potential-like channel mediates synaptic transmission in rod bipolar cells. *J. Neurosci.* 29, 6088–6093. doi: 10.1523/jneurosci.0132-09.2009

Singer, J. H., and Diamond, J. S. (2003). Sustained Ca2+ entry elicits transient postsynaptic currents at a retinal ribbon synapse. *J. Neurosci.* 23, 10923–10933. doi: 10.1523/jneurosci.23-34-10923.2003

Sinha, R., Siddiqui, T. J., Padmanabhan, N., Wallin, J., Zhang, C., Karimi, B., et al. (2020). LRRTM4: A novel regulator of presynaptic inhibition and ribbon synapse arrangements of retinal bipolar cells. *Neuron* 105, 1007–1017.e1. doi: 10.1016/j.neuron.2019.12.028

Stockton, R. A., and Slaughter, M. M. (1989). B-wave of the electroretinogram. A reflection of ON bipolar cell activity. *J. Gen. Physiol.* 93, 101–122. doi: 10.1085/jgp.93.1.101

Tachibana, M. (1999). Regulation of transmitter release from retinal bipolar cells. *Prog. Biophys. Mol. Biol.* 72, 109–133. doi: 10.1016/s0079-6107(99)00003-6

Tom Dieck, S., and Brandstätter, J. H. (2006). Ribbon synapses of the retina. *Cell Tissue Res.* 326, 339–346. doi: 10.1007/s00441-006-0234-0

Vaegan and Millar, T. J. (1994). Effect of kainic acid and NMDA on the pattern electroretinogram, the scotopic threshold response, the oscillatory potentials and the electroretinogram in the urethane anaesthetized cat. *Vision Res.* 34, 1111–1125. doi: 10.1016/0042-6989(94)90294-1

Vardi, N., Duvoisin, R., Wu, G., and Sterling, P. (2000). Localization of mGluR6 to dendrites of ON bipolar cells in primate retina. *J. Comp. Neurol.* 423, 402–412.

von Gersdorff, H., and Matthews, G. (1997). Depletion and replenishment of vesicle pools at a ribbon-type synaptic terminal. *J. Neurosci.* 17, 1919–1927. doi: 10.1523/jneurosci.17-06-01919.1997

von Gersdorff, H., Vardi, E., Matthews, G., and Sterling, P. (1996). Evidence that vesicles on the synaptic ribbon of retinal bipolar neurons can be rapidly released. *Neuron* 16, 1221–1227. doi: 10.1016/s0896-6273(00)80148-8

Wachtmeister, L. (1998). Oscillatory potentials in the retina: what do they reveal. *Prog. Retinal Eye Res.* 17, 485–521. doi: 10.1016/s1350-9462(98)00006-8

Wakeham, C. M., Ren, G., and Morgans, C. W. (2020). Expression and distribution of trophoblast glycoprotein in the mouse retina. *J. Comp. Neurol.* 528, 1660–1671. doi: 10.1002/cne.24850

Wakeham, C. M., Wilmarth, P. A., Cunliffe, J. M., Klimek, J. E., Ren, G., David, L. L., et al. (2019). Identification of PKCα-dependent phosphoproteins in mouse retina. *J. Proteom.* 206:103423. doi: 10.1016/j.jprot.2019.103423

Xiong, W.-H., Pang, J.-J., Pennesi, M. E., Duvoisin, R. M., Wu, S. M., and Morgans, C. W. (2015). The Effect of PKCα on the Light Response of Rod Bipolar Cells in the Mouse Retina. *Investig. Ophthalmol. Visual Sci.* 56, 4961–4974. doi: 10.1167/iovs.15-16622

Xu, Y., Dhingra, A., Fina, M. E., Koike, C., Furukawa, T., and Vardi, N. (2012). mGluR6 deletion renders the TRPM1 channel in retina inactive. *J. Neurophysiol.* 107, 948–957. doi: 10.1152/jn.00933.2011

Zanazzi, G., and Matthews, G. (2009). The Molecular Architecture of Ribbon Presynaptic Terminals. *Mol. Neurobiol.*39, 130–148. doi: 10.1007/s12035-009-8058-z

Zhao, Y., Malinauskas, T., Harlos, K., and Jones, E. Y. (2014). Structural Insights into the Inhibition of Wnt Signaling by Cancer Antigen 5T4/Wnt-Activated Inhibitory Factor 1. *Structure* 22, 612–620. doi: 10.1016/j.str.2014.01.009

Zhou, Z.-Y., Wan, Q.-F., Thakur, P., and Heidelberger, R. (2006). Capacitance Measurements in the Mouse Rod Bipolar Cell Identify a Pool of Releasable Synaptic Vesicles. *J. Neurophysiol.* 96, 2539–2548. doi: 10.1152/jn.00688.2006